AD-A033 624 AIR FORCE GEOPHYSICS LAB HANSCOM AFB MASS F/G 17/9
THE USE OF DIGITAL RADAR IN SHORT-RANGE FORECASTING.(U)
AUG 76 H S MUENCH, W E LAMKIN
UNCLASSIFIED AFGL-TR-76-0173 NL

1 OF 1
AD A033624

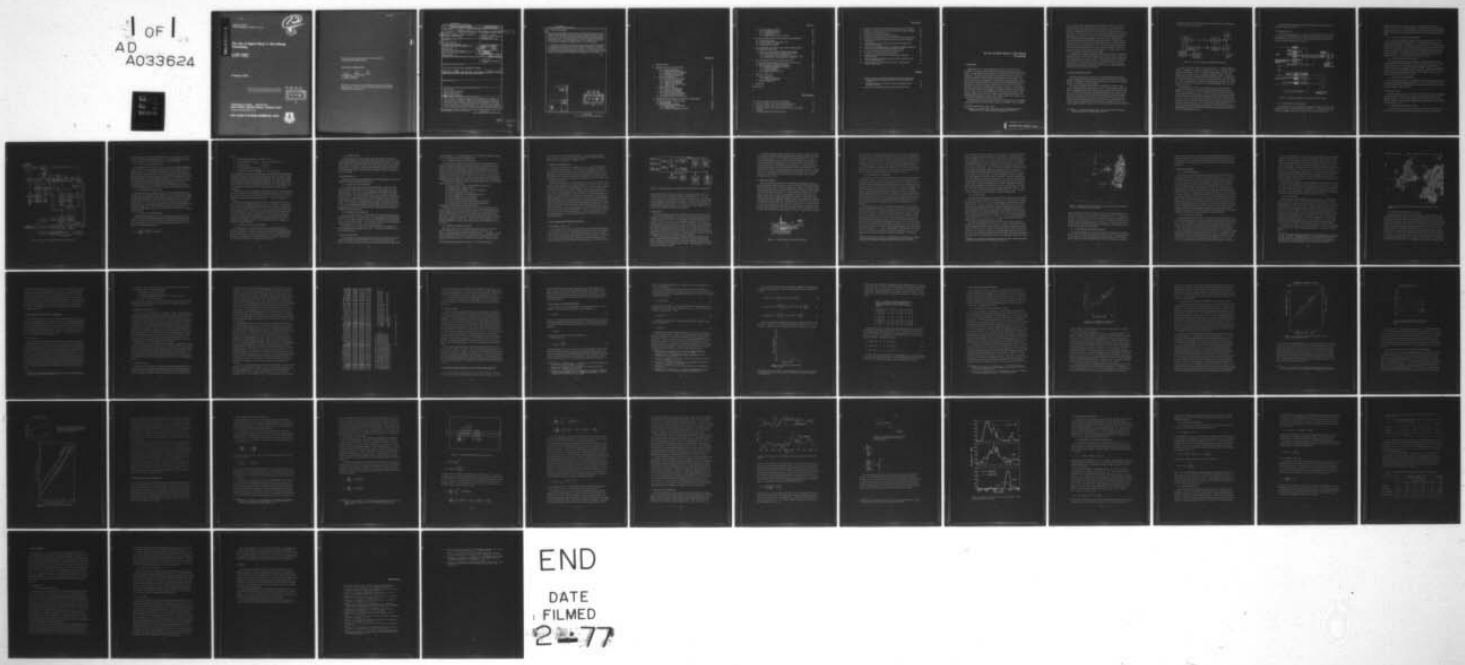

END
DATE FILMED
2-77

AFGL-TR-76-0173
AIR FORCE SURVEYS IN GEOPHYSICS, NO. 348

The Use of Digital Radar in Short-Range Forecasting

H. STUART MUENCH
WILLIAM E. LAMKIN

4 August 1976

METEOROLOGY DIVISION PROJECT 8628
AIR FORCE GEOPHYSICS LABORATORY
HANSCOM AFB, MASSACHUSETTS 01731

AIR FORCE SYSTEMS COMMAND, USAF

This technical report has been reviewed and is approved for publication.

FOR THE COMMANDER:

John Howard

Chief Scientist

Qualified requestors may obtain additional copies from the Defense Documentation Center. All others should apply to the National Technical Information Service.

Unclassified

SECURITY CLASSIFICATION OF THIS PAGE (When Data Entered)

REPORT DOCUMENTATION PAGE	READ INSTRUCTIONS BEFORE COMPLETING FORM
1. REPORT NUMBER AFGL-TR-76-0173 (9) Air Force Surveys in Geophysics,	3. RECIPIENT'S CATALOG NUMBER
4. TITLE (and Subtitle) (6) THE USE OF DIGITAL RADAR IN SHORT-RANGE FORECASTING	5. TYPE OF REPORT & PERIOD COVERED Scientific. Interim.
	6. PERFORMING ORG. REPORT NUMBER AFSG No. 348
7. AUTHOR(s) (10) H. Stuart Muench William E. Lamkin	8. CONTRACT OR GRANT NUMBER(s)
9. PERFORMING ORGANIZATION NAME AND ADDRESS Air Force Geophysics Laboratory (LYU) Hanscom AFB Massachusetts 01731	10. PROGRAM ELEMENT, PROJECT, TASK AREA & WORK UNIT NUMBERS 62101F (16) 86281103 (17) 11
11. CONTROLLING OFFICE NAME AND ADDRESS Air Force Geophysics Laboratory (LYU) Hanscom AFB Massachusetts 01731	12. REPORT DATE (11) 4 Aug 1976
	13. NUMBER OF PAGES 58 (12) 60 pp.
14. MONITORING AGENCY NAME & ADDRESS(if different from Controlling Office)	15. SECURITY CLASS. (of this report) Unclassified
	15a. DECLASSIFICATION/DOWNGRADING SCHEDULE

16. DISTRIBUTION STATEMENT (of this Report)

Approved for public release; distribution unlimited.

(14) AFGL-TR-76-0173, AFGL-AFSG-348

17. DISTRIBUTION STATEMENT (of the abstract entered in Block 20, if different from Report)

18. SUPPLEMENTARY NOTES

19. KEY WORDS (Continue on reverse side if necessary and identify by block number)

Weather radar
Radar-weather relationships
Short-range forecasting
Objective forecasting
Digital radar forecasting

20. ABSTRACT (Continue on reverse side if necessary and identify by block number)

As part of a program to improve short-range forecasts of weather conditions at aircraft terminals, a digital radar system was established at Air Force Geophysics Laboratory, Bedford, Mass. The system, consisting of AN/FPS-77, digital interface, microwave transmitter-receiver, video integrator and computer, was installed in late 1972. Since that time the system has been used in conjunction with a network of 26 automated weather stations to make experimental forecasts of visibility and severe-weather conditions. →

DD FORM 1 JAN 73 1473 EDITION OF 1 NOV 65 IS OBSOLETE

Unclassified

SECURITY CLASSIFICATION OF THIS PAGE (When Data Entered)

409 578
bpg

20. Abstract (Continued)

The radar output of digital maps of radar intensity was found to be very convenient, but the inability of the radar to detect small water droplets limits the use in low visibility forecasting primarily to heavy rain storms and snow storms. In severe storms modest success was attained forecasting gusts, using digital maps. The large amounts of weather information from the network and radar frequently saturated the forecaster making forecasts at 15-min intervals, and relief was sought in the form of objective aids.

Preliminary relationships between radar intensity, extinction coefficient (visibility) and rainfall rate have been formulated. In addition, a technique was developed using digital radar maps to obtain motion vectors and make probability forecasts of severe weather conditions. The calibration procedure relies on intensity of ground targets (hills and towers) for day-to-day relative calibration, and absolute calibration has been limited to Z-R relations.

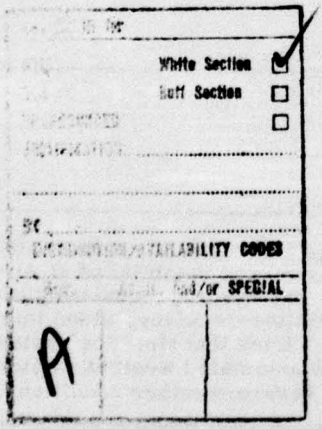

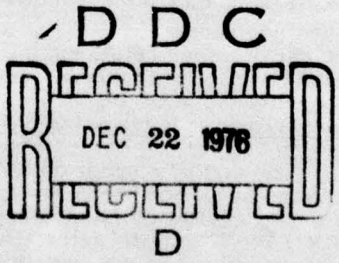

Contents

Contents

Illustrations

Illustrations

Tables

The Use of Digital Radar in Short-Range Forecasting

1. INTRODUCTION

Beginning in 1972, a major effort has been under way at the Air Force Geophysics Laboratory to improve short-range forecasts of airfield weather conditions, by exploiting recent developments in communications and data-processing technology. The principal approach has been through the deployment of some twenty-six automatic weather stations around Hanscom Air Force Base, with a spacing of about one to ten kilometers.[1] By frequently interrogating this "meso-net" of stations through a dedicated computer, one is able to follow the motion and development of many of the small-scale features that are associated with low visibility, wind squalls, and other weather hazards. However, it was recognized that the network would have limitations, and weather disturbances such as heavy showers would at times move through gaps in the network, undetected. For this reason, an effort was made to make weather radar information available to the experimental forecasters, to determine how useful the information could be, and to find how the information might best be presented.

Radar has been used as a forecast aid for more than thirty years. Throughout most of this period the principal output has been a CRT display, which is studied

(Received for publication 3 August 1976)

1. Hering, W.S., Muench, H.S., and Brown, H.A. (1972) Mesoscale forecasting experiments, Amer. Met. Soc. Bulletin, 53:1180-1183.

by a radar observer in order to determine the location, intensity, and motion of the precipitation echoes. Unfortunately, this procedure is very subjective and does not easily yield parameters (numbers) to develop into objective forecast techniques. Within the past ten years there has been a data processing revolution, and it is now practical to convert an analog radar signal to digits and process the information in a computer in real-time. So far the principal application of this new technology has been in hydrology[2] as the radar return is quantitatively related to precipitation rate and the excellent resolution and coverage of radars make forecasts of run-off and stream flow feasible. However, many other applications should now be possible, as the radar return is also related to visibility and to severe weather parameters such as hail and wind squalls. Thus there is good reason to believe that computer-radar systems or "digitized radar" will soon prove useful in aviation terminal forecasting.

A program was set up in conjunction with the mesonet program to exploit the potentials of radar in terminal forecasting. First a digitized radar system would be set up and tested, then, radar-weather relationships and forecast techniques would be developed from digital radar data. Finally, techniques would be tested and evaluated. This report is intended to describe the radar system that was assembled and present some preliminary results of radar-weather relationship studies and forecast technique development.

2. MESONET DIGITAL RADAR SYSTEM

When the mesonet project was set up, a Honeywell HW324 dual-processor computer system was made available and installed at the mesonet forecast operations site. To provide radar information we would need a radar set, a recording system, and an interface with the computer.

The radar set attached to the system is an AN/FPS-77 C-band (5.35 cm) radar, located on the flight line of Hanscom AFB. When the project started, this radar was being used for routine radar observations by the Base Weather Station (Det. 6, 6th WWG), but since these observations took only a few minutes of each hour, there was ample time available for gathering data for research purposes. However, this did mean that we needed a means to tap into the receiver and to transmit the data 1500 meters to the AFGL computer and a means to share the control of the radar with the Base Weather Station. In addition, we would need remote scopes to monitor the radar, as well as the previously mentioned recording

2. Wilson, J.W. (1970) Integration of radar and rain gauge data for improved rainfall measurement. J. Appl. Met. 9:489-497.

and interface systems. The basic features of the system that was constructed are shown schematically in Figure 1.

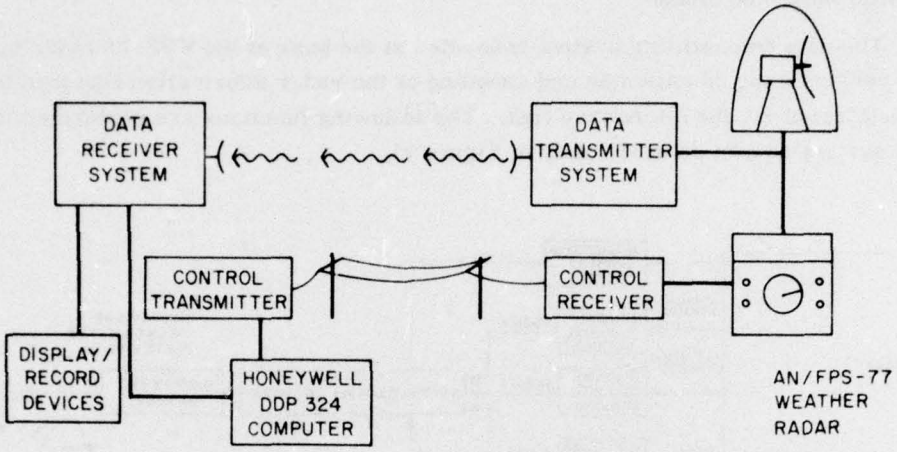

Figure 1. Schematic Diagram of Mesonet Radar System

In order to avoid the pitfalls of analog transmission, a completely digitized system was designed and constructed by Raytheon Company. The system provides radar data transmission and remote control through a hybrid microwave and telephone link. Digitized radar video signal, magnetron current, and antenna position information are multiplexed into a serial "bit stream" and transmitted via a microwave system to the "remote" mesonet forecast site. Since the signals for remote control purposes (switching and changing antenna position and magnetron current) require little bandwidth, unconditioned telephone lines, driven by modems, are used.

Modifications to the FPS-77 were required in order to interface the two systems. A solid-state mixer having two output ports replaced the standard FPS-77 mixer. One port matches the output of the normal mixer and feeds the conventional receiver in the console. The other port provides the proper signal to drive a high precision solid-state logarithmic amplifier (90dB-dynamic range, ±0.5-dB accuracy). Further wiring modifications were made to the console portion of the radar to permit the control function to be switched between the console and the mesonet operation site. At the mesonet site, standard PPI and RHI scopes were installed and outfitted with periscopic camera hoods, while equipment was brought in to interface the received data both with the HW-324 computer and the Ampex FR2000A tape recorder.

In the following sections, the basic four sub-systems as shown in Figure 1 will be described in more detail.

2.1 Data Transmitting System

The data transmitting system is located at the base of the FPS-77 radar tower and performs the conditioning and encoding of the radar information required for transmission via the microwave link. The following functions are performed in this system (shown schematically in Figure 2).

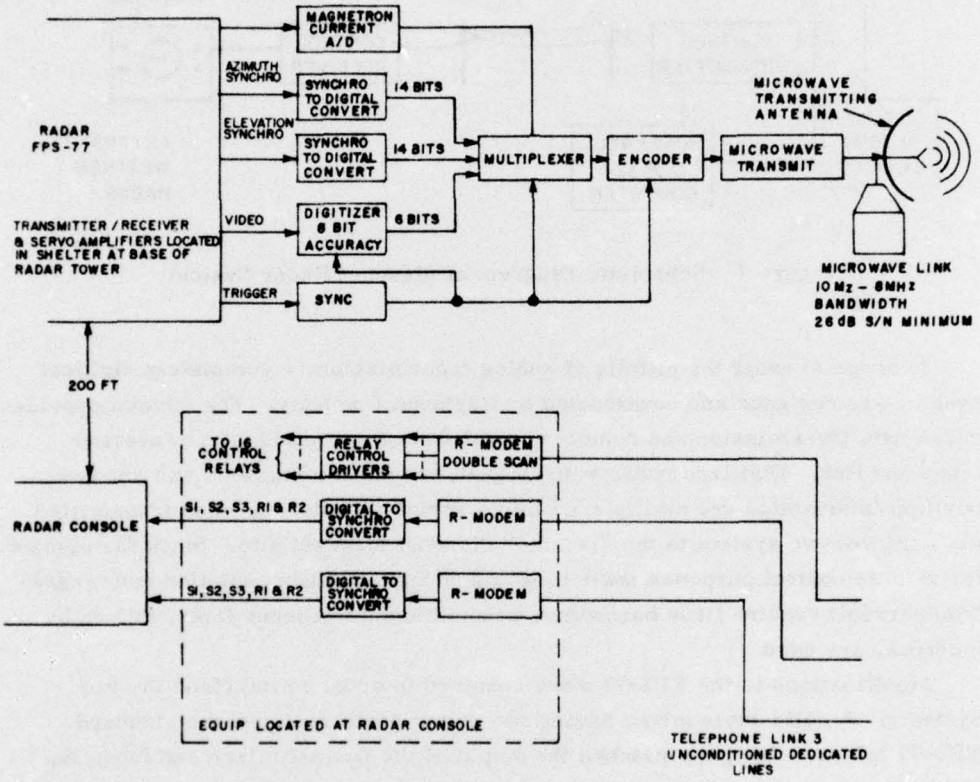

Figure 2. Schematic Diagram of the Data Transmitting System

2.1.1 VIDEO SIGNAL CONDITIONING

The output of the precision logarithmic amplifier is adjusted by means of two front panel switches. The dB/volt switch (calibrated in 0.1-dB steps) is provided to match the logging characteristics of the receiver with the Digital Video

Integrator that interfaces with the computer. The second switch is an offset control to correct for any dc offset voltage that may occur on the video line. This control can also be used to bias the nonlinear low level response of the logarithmic amplifier below the level of the analog-to-digital converter's minimum detectable signal.

2.1.2 ANALOG-TO-DIGITAL CONVERSION

The conditioned video signal is converted to 6-bit binary numbers in a high-speed analog-to-digital converter (A/D) that is sampled every two μsec by a sample-and-hold amplifier. The output is on six parallel lines. This allows video numbers from 0 through 63, providing a resolution of 1.5dB, and a maximum value of 94.5dB. Signals from both the azimuth and elevation synchro's are converted to 14-bit numbers in two synchro-to-digital converters (S/D), providing a resolution of 0.02 degrees. The magnetron current is converted to a 6-bit number in another A/D converter, with a resulting resolution of 0.5 mA.

2.1.3 MULTIPLEXING AND ENCODING

The multiplexer-encoder uses shift registers to change the parallel input signals into a serial "bit" stream for the microwave transmitter. Upon receipt of a radar trigger pulse, a 30-bit code sequence is generated, followed by the azimuth, elevation, and magnetron current information. Then comes a continuous stream of 1200 six-bit video signal values. Timing is controlled by a 3-MHz clock, which is asynchronous with the radar trigger. The 3-MHz rate is dictated by the six bits of radar video every two μsec.

2.1.4 MICROWAVE TRANSMITTER

The microwave transmitter is a solid-state, FM system operating at 1.76GHz, with a bandwidth of 8MHz (though only 3MHz is used). The transmitter is located at the base of the radar tower and feeds the antenna located about 28 meters above through a flexible coaxial wave guide.

2.2 Data Receiving System

The data receiving system decodes the received microwave signals, managing and transforming the information as required by the peripheral devices such as the tape recorder, remote scopes and digital readout, as well as the Honeywell DDP324 computer. The following paragraphs describe this system, which is shown schematically in Figure 3.

2.2.1 MICROWAVE RECEIVER SYSTEM

The receiving antenna is located on the roof of a building in the AFCRL complex, about 1.5 km south of the transmitting antenna, and the received signal

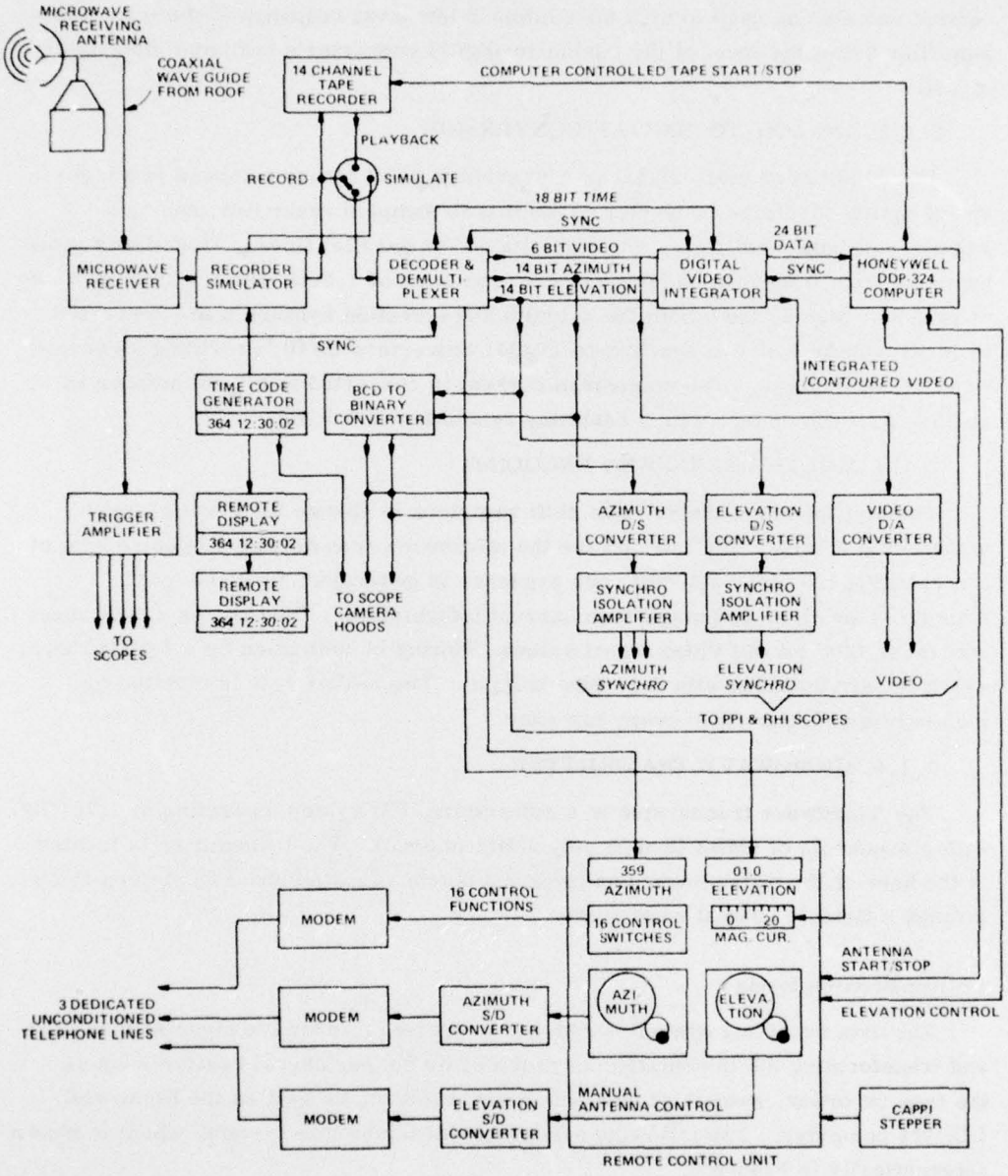

Figure 3. Schematic Diagram of the Data Receiving System

travels by flexible coaxial waveguide approximately 85 meters to the solid-state receiver, located in the "Mesonet radar room". The output from the microwave receiver is identical to the bit-stream that went into the transmitter.

2.2.2 DATA RECORDER/SIMULATOR

The data output of the microwave receiver is fed into the Recorder/Simulator chassis, which acts as an interface between the tape recorder system and the data receiver system. A "record/reproduce/simulate" switch allows the operator a choice of three modes of operation. In the "record" position, unprocessed radar data plus data from the system digital clock are sent both to the tape recorder and to the demultiplexer-decoder (for further processing). In the "reproduce" position, the data stream from the microwave receiver is shut off and in its place data from the tape recorder flows into the decoder-demultiplexer, and drives a "re-play" display clock. The "simulate" mode allows adjustable bit patterns to be fed into the system in place of real data to check the data converting circuitry.

2.2.3 DECODER-DEMULTIPLEXER

This unit contains the necessary circuitry to decode and demultiplex the incoming serial data, to regenerate the 3-MHz clock, and to provide parallel outputs of video signal, azimuth and elevation position, magnetron current, radar trigger, and range-gate clock pulse. The 3-MHz clock is regenerated and held in place by analysis of the received serial bit stream (which is artificially prevented from becoming "quiet"), and provides the timing to remove data from the shift registers into parallel output lines. The parallel data are then fed to the Digital Video Integrator, to digital-to-analog devices to drive the remote scopes, and to digital readout displays.

2.2.4 DIGITAL VIDEO INTEGRATOR

The Digital Video Integrator (DVI) is a solid-state signal processor, manufactured and modified by Raytheon Company, that integrates (at constant range) video data, adds a range-normalization value and transmits azimuth, elevation, time, and integrated video data to the Honeywell DDP324 upon request. The DVI performs the following computation:

$$\overline{V} = \frac{1}{I} \sum_{i=1}^{I} V_i \left(\frac{N-1}{N}\right)^i + \frac{K}{8} \log_2 R^2$$

where:

V is the video signal (units of 1.5 dB) $0 \leq V \leq 63$,

N is integration "time constant" $1 \leq N \leq 2^{13}$, $2^0 \leq 2^N \leq 2^{13}$,

R is range number $0 \leq R \leq 1200$,

K is normalization slope factor $0 \leq K \leq 15$,

I is the point at which $Vi, R \left(\frac{N-1}{N}\right)^i \rightarrow 0$, due to truncation.

The computation is accomplished in two stages, so two sets of 20-bit shift registers are used for temporary storage of information at each of the 1200 ranges. Range normalization values are permanently stored within the DVI. The "K" value used matches characteristics of the precision log amplifier. The purpose of the range normalization process is to compensate for signal loss due to beam divergence as range increases. With the radar beam filled uniformly with precipitation particles, the radar return will decrease at $1/R^2$ as the range increases (assuming no absorption).

Upon receipt of a request signal from the Honeywell DDP324, the DVI transmits up to 1200, 24-bit "words" over parallel output lines at the rate of 500,000 words-per-second. The first three words contain azimuth, elevation, and time data, and the remaining words each contain the six bits of rad data and a range cell number.

The DVI also serves to provide "quantized" video information for use in the remote scopes. The integrated digital video values are converted to analog signals and compared with six thresholds (each set to one of 32 values) and converted to a level which produces black, gray, or white on the scopes, depending on the setting of seven toggle switches. (This DVI was, in fact, originally built for this purpose, and later modified to interface with the DDP324.) The resulting output provides "contours" on the remote PPI and RHI scopes, that can be interpreted quantitatively in terms of dB level. The role of the integrator in this operation is to smooth out "meteorological noise" in the radar signal so that the "contours" are smoother and more persistent.

2.2.5 DIGITAL TO ANALOG CONVERSION

Two digital-to-synchro converters (S/D) accept parallel output from the decoder-demultiplexer and provide azimuth and elevation synchro signals to drive the PPI and RHI scopes. A digital-to-analog converter (D/A) changes digital video information (not integrated) to an analog signal as an alternate source for PPI and RHI display. Another D/A converter is attached to the magnetron current lines and the output is connected to a milliampere display meter.

2.2.6 SYSTEM CLOCK

A Systron-Donner 8120 digital clock system was installed to synchronize clock timing throughout the recording and display units of the system. The master clock is located in an instrumentation rack in the Mesonet radar room, one "slave" unit is located in the Mesonet computer room, and a second unit is in the Mesonet forecast room. In addition, binary-coded-decimal (BCD) outputs are tied to the Recorder/Simulator unit, to the Digital Video Integrator and to LED displays in the camera hoods.

2.3 Display/Record Devices

Several devices are used to display and record radar information. These are physically located in the Mesonet radar room.

2.3.1 MAGNETIC TAPE RECORDER

A 14-channel Ampex tape recorder (model FR2000A) is used to record the basic bit-stream output of the microwave receiver, to which digital clock data have been added. A 1-in. (2.54-cm), high quality instrumentation tape records the 3-MHz signal, with the tape moving at 120 in./sec (3.048mps), on a single channel at a time. At the end of the tape, fifteen minutes later, the tape reverses and records in the opposite direction on an adjacent channel, and so on, until all channels have been used, which allows about 3.5 hours of continuous recording to a tape. To allow longer recording between tape changes, control and sense lines are connected to the Honeywell DDP324, so that a program can automatically turn the tape unit on and off. If 40 seconds of data are recorded every five minutes, a single tape will last 26 hours.

2.3.2 REMOTE SCOPE DISPLAYS

For remote display, there are three AN/GPA 127 PPI scopes (originally built for AN/FPS-3 radars). Two of the scopes can be photographed on either Polaroid film or on 35-mm film (Fairfield 015 cameras). This duplication in scopes allows recording at two different ranges. The third PPI is used for visual monitoring and manual tracking of radar echoes, in the traditional manner.

In addition, there is a modified CPS-9 Remote RHI scope, mounted in an FPS-3 housing and also equipped with camera. This is used to monitor the vertical structure of storms.

2.4 Remote Control of the FPS-77

A control system was assembled so that personnel in the Mesonet radar room could have complete control of the FPS-77, or could transfer control to the FPS-77 console when required for routine Base Weather Station radar observations,

or for maintenance. The control functions are accomplished by digital data transfer over unconditioned, dedicated telephone lines.

2.4.1 REMOTE CONTROL TRANSMITTER

At the heart of the transmitter are three 16-bit Larse Data Communication modems contained in the FPS-77 Remote Control Unit. Two handwheels drive synchro-to-digital converters (similar to those in the Multiplexer-Decoder) and output 14-bit words, representing commands for azimuth and elevation angles. Each set of 14 parallel output lines feeds into a modem (Larse LCS-151-55) which converts the parallel data to an FSK-encoded serial bit stream and transmits at 360 bits/sec, over a dedicated line. There is also an option to have the Honeywell DDP324 generate the azimuth and elevation commands and by-pass the handwheels.

The third modem transmits control switch position information. The following control functions are represented:

(1) Master Control - FPS-77 console/Mesonet radar room,
(2) Emergency power shutoff, FPS-77,
(3) Emergency power shutoff, microwave transmitter,
(4) FPS-77 transmitter power on/off,
(5) FPS-77 transmitter re-set (push button switch),
(6) FPS-77 Magnetron current raise/hold,
(7) FPS-77 Magnetron current lower/hold,
(8) Azimuth control continuous rotation/remote positioning*,
(9) Elevation control automatic RHI/remote positioning*.

Seven additional functions have remained unspecified.

These sixteen control-switch position data are also FSK-encoded in a Larse modem (model LCS-151-31) and transmitted serially over the third telephone line. Incorrect signals for the emergency switch positions could cause great inconvenience and radar data loss, so, to ensure reliability, the control modem uses a double scan – at the receive end, two consecutive identical words must be received before the output function is activated. Theoretically, if the telephone line noise is within specification, a serious error should not occur more often than once in 10^8 years.

2.4.2 REMOTE CONTROL RECEIVER

The remote control receiver is physically located adjacent to the FPS-77 console. Within this receiver are three modems (two LCR-251-55, one LCR-151-31) complementing the three transmitting modems. Each modem decodes an FSK encoded serial bit stream and produces output on 16 parallel lines. The azimuth and elevation lines are each connected to a digital-to-synchro converter,

*Remote positioning by handwheel, computer, or CAPPI stepping switch.

the output of which is used to position the radar, if the control switch for that function permits. The control lines outputs are connected to relays within the FPS-77 console to perform their assigned functions.

2.5 Completion Schedule and Maintenance

The basic transmitting and receiving systems were developed by Raytheon, Inc., installed during the summer of 1972 and become operational in October of 1972, one month after the mesonet stations and data presentation system became operational. The Ampex tape recording system was installed in July 1973, along with the Recorder/Simulator unit and the system digital clock. Modifications to allow computer control of antenna position and stop-start of the tape recorder were completed by October 1973.

As might be expected with a fairly complex electronic system, there are some weak links, and outages due to component failures occur from time to time. Perhaps the biggest problem has been keeping the FPS-77 itself operational. Problems with the FPS-77 arise almost weekly, though, fortunately most of these can be corrected in a couple of hours or less by replacing an expendable part (crystal or tube). Many of the minor failures appear to be due to line power fluctuations. On several occasions, principally in 1974 and 1975, major problems developed that halted operations for several weeks at a time, for example, slip ring replacement and pedestal replacement. The Ampex tape recorder has failed on several occasions, and being a precision instrument (recording density 25,000 bits/in.) repairs must be made under contract, a procedure usually taking several weeks. Fortunately this recorder is not crucial to operations. Of the remaining electronics, the only major problem has been with the digital-to-synchro converters which fail two to three times a year (reason still unknown). In spite of these problems, the system (excluding Ampex recorder) has been operable about 85 percent of the time since October 1972.

3. COMPUTER PROGRAMMING FOR DIGITAL RADAR MAPS

3.1 Mesonet Project Computer System

The computer system that was made available for the mesonet forecast project for real-time experiments is a Honeywell DDP 324 dual processor (see Figure 4). Each of the two data processors uses 24-bit data words, has access to 24,000 words of private memory and shares 8000 words of common memory. The processors also share the peripheral input-output devices, which include paper-tape punch and reader, punch card reader, two line-printers (one a stand-by), and two

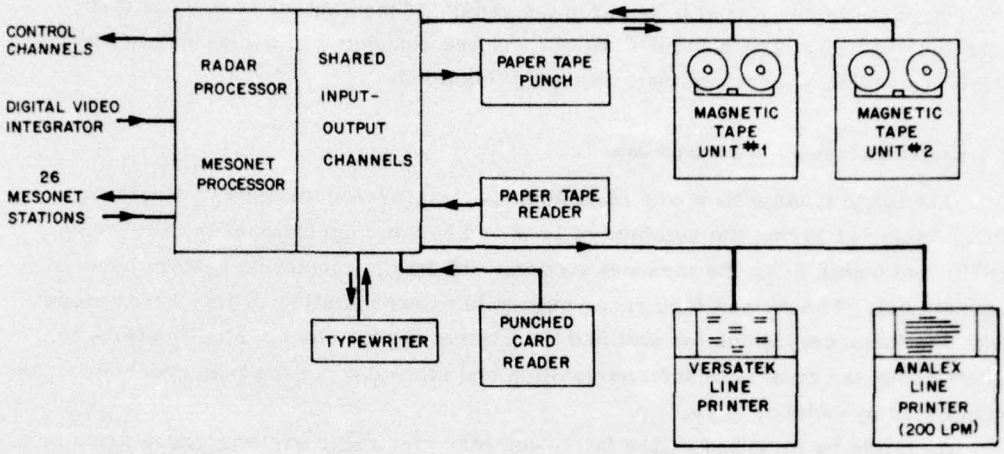

Figure 4. Schematic Diagram of the Honeywell DDP 324 Data Processing System

magnetic tape drives. By modern standards, the processors are not fast: the cycle time is 1.75 μsec, with add, multiply, and divide times of 3.5, 14, and 19 μsec, respectively. The arithmetic hardware is all fixed point. The computer has been programmed using assembly-language, a more laborious procedure than using FORTRAN, but well suited for our needs in a real-time situation with non-standard input-output data channels. The limitations of computer speed and memory size were important factors in program design.

3.2 Radar Displays

The most convenient form of radar presentation for forecaster use is a horizontal map, periodically updated. In the past, such maps have been generated on a cathode-ray tube (CRT) which has a rotating beam representing the radar beam, and which "paints" a picture as the radar antenna rotates about a vertical axis, pointing near the horizon (referred to as "PPI" presentation). There always have been difficulties working with such CRT displays that would be overcome by obtaining "hardcopy" (paper) maps that portrayed both pattern outline and radar intensity values. Paper maps are very convenient to a forecaster as he can easily scan back and forth in time to study motions. Intensity information is vital for detecting development as well as for constructing forecast techniques.

There are several ways in which a computer can be used to generate radar maps. Perhaps the most ideal would be to have the maps drawn by a "plotter" device. Contours of intensity would be drawn along with labels, legends and additional information such as weather station locations. Unfortunately, our computer did not come with such a plotter.

A quicker, though less elegant, procedure is to have the computer utilize the line-printer and print characters representing radar signal intensity at each point in a grid of data points. From a distance, the characters appear to merge, to form continuous patterns similar to those on the CRT display, and close up, they can be inspected to give intensity and cell size information. Intensity labels would be unnecessary, and legends are easily printed. For station locations one uses plastic overlays, which are also useful for transferring information from chart to chart to deduce motion and development. The printed maps are, of course, convenient for archiving, though bulkier than the traditional 35-mm films of CRT displays, and the digital data can be easily stored on magnetic tape for further processing at a later date.

3.3 Program Design, RADAR I

The radar information received from the Digital Video Integrator (DVI) is in spherical coordinates (see Figure 5) and must be converted to cartesian coordinates for the printed map output – a problem in geometry. Actually, one need only multiply the range by the sine of the azimuth, the cosine of the azimuth, and the tangent of the elevation angle to obtain the X, Y, and Z coordinates, respectively. Of course, there is not a one-to-one correspondence of radar values received and points in an X-Y grid, so further processing is necessary. A single radar pulse returns data from 1200 "range bins," each of which basically represents a segment of a long, thin cone (see Figure 5). These segments are each 300 meters long, but of a diameter that varies from 10 km at maximum range (360 km) to only 30 meters at 1 km. This means that the radar "bins" are much smaller close in than far out, and also that the samples are from different heights. Ideally we would like to have the output map represent a horizontal surface. Further, the map would be composed

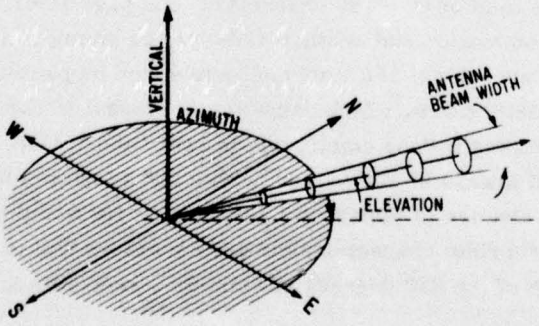

Figure 5. Coordinate System for Radar Information

of a large number of squares, and the radar value for each square would be representative of the average value throughout the area of the square. Unfortunately, the data flow rate from the radar is simply too fast to construct an "ideal" map in real time. Data from the DVI are brought in on the direct-memory-access channel (DMA), operating in the "hog mode." In this mode, the computer goes into "suspended animation" as a batch of 1200 radar words is brought directly into memory in a 2400 μsec data burst. Only 686 μsec later, radar data from the next pulse are ready, and this is obviously too little time to process 1200 data words when the fastest arithmetic operation – add – requires 3.5 μsec.

3.3.1 ENGINEERING COMPROMISES

Of necessity, a number of compromises were made when the first operational program was written. To save precious time, the range is limited to 640 bins, equivalent to 192 km (104 nmi), and requiring only 1280 μsec for input. Next, only radar data nearest to every degree of azimuth are used, representing about every 14th pulse. This is a sensible compromise as the beam width is 1.6 degrees wide and data taken at intervals of less than one degree are really not independent. In addition, the DVI can be set to perform a running time integration, at constant range, (described in 2.2.4) that is useful in smoothing out "meteorological noise."* With the DVI selector switch set at "16" one obtains a time integration that is compatible with the FPS-77. So, by reducing range and sampling frequency the data flow is reduced to 640 words every 42,000 μsec, thus providing about 75 μsec to process each word of data – sufficient time for some processing but hardly generous.

The time problem was further simplified by assuming that the radar value from the available range bin nearest the center of the grid square would be representative of that square. This assumption eliminates the task of averaging all data that fall in each square, saving time as well as considerable amounts of storage. In fact, for a single map of 60 × 120 characters (our page size) 7200 words would be needed for the summation and another 7200 for the number in the summation. Without the spatial averaging, the 7200 characters can be packed in 1800 words. The actual task of determining which range bin is closest to the center of a square could be time consuming if done completely in real time. Also, it would be redundant in that it would always be the same azimuth and range bin for the same square. This would suggest the use of tables. Unfortunately, we would need some 230,000 words to store appropriate character numbers corresponding to each of the 640 range-bins for each of the 360 degrees of azimuth – reducible to 115,000 with

---

*"Meteorological noise" is the series of high frequency fluctuations in the returned signal that is generally attributed to rapid changes in shape, orientation, size, and number of the larger precipitation particles that dominate the return.

packing, but still a prohibitive number. As an alternative, the program considers only every other range-bin, and a table of 115,000 (320 × 360) one-bit words is packed into 4800 computer words. Each of the one-bit words indicates whether or not that range-bin is a bin closest to the center of some square. At each degree of azimuth the program scans the appropriate 320 one-bit words, and for those that are a "1," a grid location is computed from the range and azimuth (sines and cosines are stored in tables). Then, four adjacent range-bins are summed (two at shorter range, one at longer range) and averaged by a two-bit register shift (equivalent to divide-by-four, but faster) and an appropriate character is stored. If the average is not greater than the range-normalization value for that range (zero radar signal) then a blank character is inserted. In this first program the maps were based on a constant elevation angle (0.5 to 1.0 degree) rather than the ideal horizontal surface or constant altitude, a procedure that also simplifies the programming. The only disadvantage to this method of map generation is that at longer ranges a single bin may overlap the center of two grid squares, and only one of them will be filled with radar data, leaving a few blanks in the map. However, this has not created any difficulties in using the maps – if it had, a routine to fill in skipped squares by interpolation would have been developed.

3.3.2 OUTPUT MAPS

The high-speed printer attached to our Honeywell computer has 10 characters/in. (3.9/cm) across the page but only 6 lines/in. (2.3/cm) down the page. Individual characters are thus in 2.54 × 4.23 mm rectangles, not the squares we would have preferred. For user convenience we decided that the scale factors in the X and Y directions should be equal, which meant the resolution in the X direction would be greater than in the Y direction, and the programming would be a little more complicated. Two maps are printed every five minutes, to be synchronized with the output from the mesonet data program. The first map is a coarse scale map (example in Figure 6) at 1 cm = 6.5 km (1 in. = 8.9 nmi), and the second map is fine scale with 1 cm = 2.16 km (1 in. = 3.0 nmi) covering only the northeast quadrant where the mesonet stations were located).

The output from the DVI represents the radar return, range-normalized, in 1.5-dB steps, with integers from 0 to 104 or 0 to 156 dB.* If we wanted to cover the entire range and use one character and only the numerals 0 through 9, then we would be limited to a 16-dB resolution – this seems much too coarse. Being more realistic, it was unlikely we would ever see anything higher than 96 dB, even with 10-cm hail stones, and there would be no point in trying to track normalized returns less than 30 dB as they would be below the limit of detectability beyond 9 km (6 nmi).

*Integers from 0 through 63 (0 through 94.5 dB) are integrated in the DVI and range normalization values of 0 to 41 (0 to 62 dB) are added.

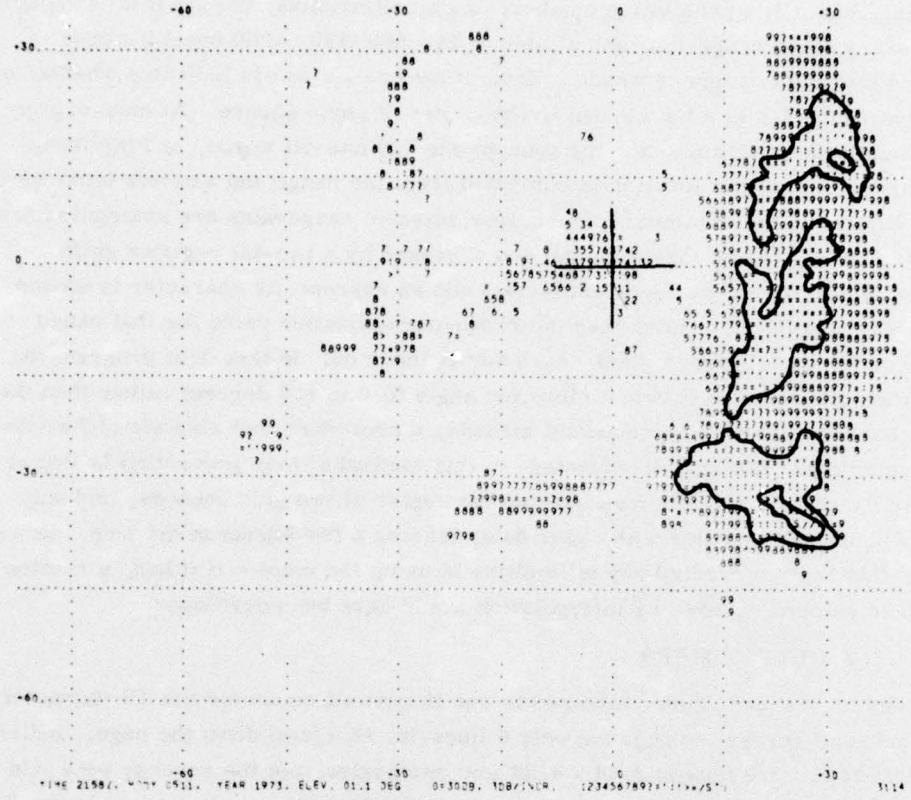

Figure 6. Example of Computer Generated Radar Map from Program RADAR I (contours were hand-drawn for emphasis)

These simplifications reduce the range to 66 dB, and for programming ease, we chose increments of 3 dB. The characters printed start with a "1" at 33 dB and step up a "9" at 60 dB. Beyond 60 dB the characters come out in accordance with the order on the print wheel, thus "?=':!>*/STU" (it was sheer coincidence that the last three letters were the programmer's nickname). We should point out that we did not have (and still don't have) a rigorous calibration – for an approximate conversion, subtract 20 dB to obtain dBZ_e.

3.3.3 PROGRAM COMPLETION AND USAGE

The program RADAR I was written and checked out during the fall and early winter of 1972-73, and became operational in February of 1973. During the following ten months, the radar and computer were used during 21 real-time visibility forecast episodes, 10 severe weather forecast cases, and 8 other data collection

cases – a total of 140 hours of operation and nearly 2000 printed digital maps archived. The computer system was operational approximately 97 percent of the time during this period, with the principal difficulty being mechanical failures in the line printer. In addition, there were no major problems with the radar during this period.

3.4 Program Design, RADAR II

3.4.1 NEW REQUIREMENTS

The first year of mesonet operations taught us much about operational forecasting on the "mesoscale." One lesson was that even in "easterly" storms the low visibility patterns were moving from the south and southwest – not moving from the ocean to the east. Thus, several stations at the northeast end of the network were dismantled and re-located to the southwest, to provide earlier warnings. The mesonet data program was rewritten to display the new stations, and, of course, the radar program would also have to be rewritten. We also found that extracting data from the radar maps by hand (for radar-weather relationships) is a laborious chore, so it was desirable to have the radar data in a more useful form for research purposes. Further, by November 1973, the Ampex tape recorder had been installed along with the computer tape controls and computer radar-position controls, and we then needed programs to utilize these controls so that fewer tape changes need be made. A new routine was needed to process data when the source was the Ampex recorder and not the radar in real-time, as the date and time information for RADAR I originates in the mesonet data processor. Finally, we needed a program with which to investigate the advantages of constant-altitude display (CAPPI) as contrasted with the constant elevation angle of RADAR I. These requirements meant writing a new and considerably more complex program.

3.4.2 A MULTI-USE PROGRAM

The program RADAR II is designed to be used in any one of three basic modes. First is the data gathering mode which is intended for use during off-hours, requiring no operator attendance. The program simply controls the Ampex tape recorder so that a 40-sec data stream is placed on the instrumentation tape once every five minutes, which would allow the tapes to last for over 24 hours without change.

The second mode of operation is the data display mode. This is a real-time data processing program which has many output options that are controlled by using sense switches located on the Honeywell DDP 324 console. Like RADAR I, maps can be printed out every five (or fifteen) minutes, synchronized with the mesonet printed data. The scale of the fine-scale map was reduced to 1 cm = 2.5 km (1 in. = 4.3 nmi) so that one map could cover all network stations. Further, the

operator can shift the origin of the X-Y axes to one of five positions to concentrate attention on a particular area. One optional output is to gather radar information directly over network stations and print out one-minute and five-minute mean values. Another option (added later) is to generate fine- and coarse-scale maps every minute and place the maps on magnetic tape (for processing on the AFGL CDC 6600 computer). This has proven to be a very useful option and is the primary means of archiving data. A third option is to have a series of three constant-altitude maps constructed every five minutes. To do this, the computer increases the elevation angle each radar revolution by 1 to 2 degrees and a stored table based on radar bin number indicates at which level (levels) the radar value of a grid point belongs. This option has not had a very high priority* and the routines have not yet been fully tested.

The third mode of operation is simply a playback from the Ampex rate recorder. In this mode, the digital maps are generated in the same manner as the data presentation mode, but time, date, and synchronization information is not obtained from the mesonet data processor. In addition, the incoming data are carefully screened to avoid the brief periods when the Ampex recorder stopped and started every five minutes, as such data contains erroneous information.

3.4.3 OUTPUT MAPS

The printed maps from RADAR II are basically the same as with RADAR I, that is, they consist of 60 rows of 120 characters of radar intensity. A minor change made was to remove the rows and columns of dots that formed a reference grid in RADAR I, as they were of little use, but leaving one row and one column through the origin to help orient overlays. Another small change made was a new set of characters and a higher threshold. While some of the weaker signals in RADAR I are of importance in snow and fine rain, following such patterns is frustrating as they soon disappear due to range attenuation. A more realistic lower threshold of 45 dB was adopted as it would allow tracking out to 50 km (30 nmi). The character sequence in 3-dB steps is "1, 23:45+67@89#XY." The non-integer characters were strategically placed to give some idea of indicated weather – "," for light rain or drizzle, ":" for moderate to heavy rain and possible hail, "@" for hail and violent squalls, and characters beyond "9" are extreme conditions (only observed from "bright" close-in ground targets). An example is shown in Figure 7.

---

*The constant altitude option is made difficult by time limitations and is tricky to "de-bug." Further, de-bugging attempts were often frustrated by major FPS-77 failures. It was also recognized that the slow rotation speed of the FPS-77 (1/14 sec) permits only 15 elevation steps in 3.5 minutes, the maximum allowable time, thus at 1.5-degree steps we only get to 23 degrees, blanking out a large part of the map at levels above 4 km (35 percent of our network).

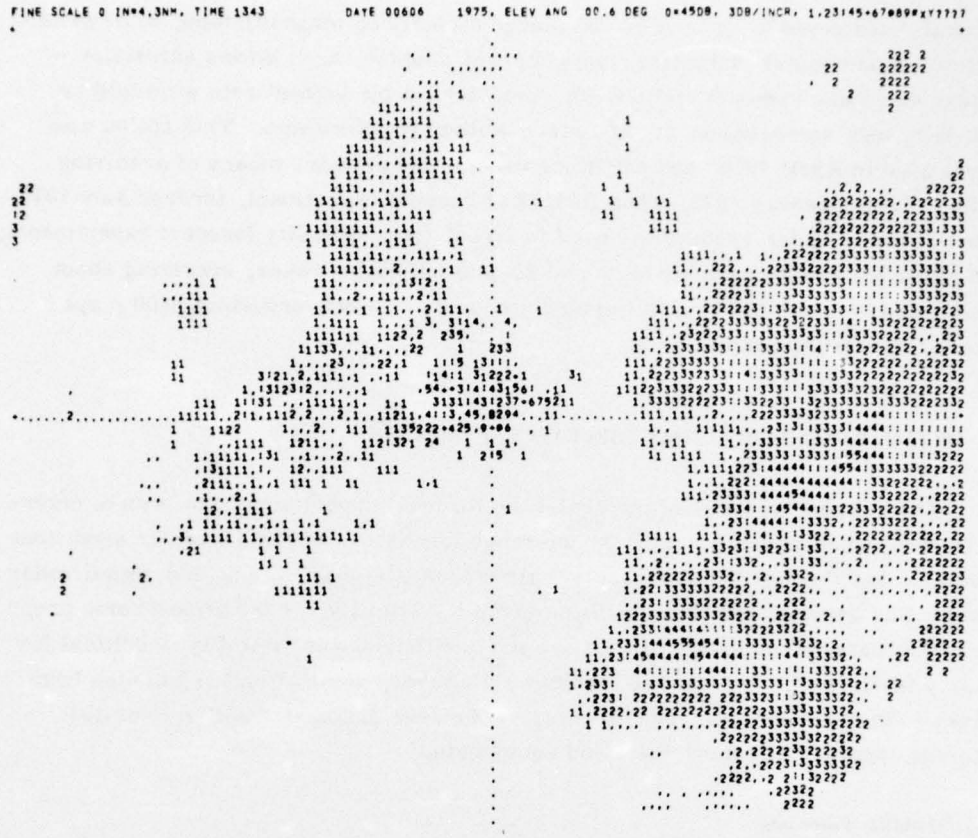

Figure 7. Example of Computer Generated Radar Map from Program RADAR II

3.4.4 PROGRAM COMPLETION AND USAGE

The RADAR II program was written during the fall of 1973 and became operational in December 1973, although some options became available at a later date. The plan for 1974 was to make real-time forecasts during normal working hours, but to record data during off-hours and run simulated real-time experiments during periods of good weather. All mesonet data were routinely placed on magnetic tape, and the Ampex tape recorder was expected to take care of the radar data, under computer control. Unfortunately, the system did not work well as power surges often halted the computer and required a manual restart, and failures developed in the Ampex recorder that were a long time in being corrected. One alternative was to use the 35-mm pictures of the radar scopes which showed contoured video data from the DVI (as described in 2.2.4). However, the films were not convenient to use even when placed in a viewer. The solution was to modify the program so that

digital maps could be generated and placed directly on magnetic tape, to be printed later. A one-minute sampling frequency was adopted, as it allows extraction of radar data near mesonet stations (by computer) at the highest rate we would be likely to use, for development of radar-weather relationships. This option was first used in April 1974, and has since become the primary means of archiving data. From January 1973, when RADAR II became operational, through July 1975, the computer-radar system was used in 2 real-time visibility forecast experiments, 10 cases for severe weather tests and 21 data collection cases, operating about 110 hours. Some 2300 maps were printed and archived, and about 6800 maps stored on magnetic tape.

4. DIGITAL RADAR IN REAL-TIME FORECAST EXPERIMENTS

The primary purpose of the real-time forecast experiments has been to determine how much improvement in short-range forecast of airfield weather conditions can be made through the use of automatic mesoscale observations and digital radar data. The greatest attention has been given to visibility, or the atmospheric property that determines visibility – extinction coefficient – as visibility is critical for safety in aircraft take-offs and landings. However, some attention has also been given to the problem of forecasting severe weather associated with convective storms, particularly wind gusts and heavy rain.

4.1 Visibility Forecasts

The visibility forecast experiments were initially set up with two forecasters making forecasts whenever there was a threat of low visibility (less than 1500 m or 1 mile) in the network. One forecaster had conventional weather data consisting of airways teletype reports, facsimile weather maps, and radar scope presentations. The second forecaster had use of the conventional data plus four maps of mesonet data and two of radar data (when needed and available) every five minutes. Forecasts were made every 15 minutes, at which time both forecasters received, as a guide, a "Markov model" forecast[3] that utilizes the latest observation of extinction coefficient, the climatological normal for the time and season and a statistically derived decay coefficient. In practice, the Markov forecast has proven an excellent control, and after the first year of forecasting the conventional forecast scores were so close to the control that the "conventional" forecast role was no longer filled.

---

3. Tahnk, W. R. (1975) Objective Prediction of Fine-Scale Variations in Radiation Fog Intensity, AFCRL-TR-75-0264, p. 10.

There were several situations in which radar information was expected to be of considerable value in visibility forecasting:

(a) visibility lowered by heavy rain,

(b) visibility varying in showery snow,

(c) visibility suddenly improving with rain "washing out" fog,

(d) new and unexpected situations.

In fog cases without precipitation, particularly radiation or ground fog, the radar maps would not be of any use, as the fog particles are simply too small to be detected by the FPS-77 radar.

4.2 Radar Benefits in Visibility Forecasts

The obvious way to demonstrate the contribution of digital radar information to forecast skill would be to conduct a series of tests in which one forecaster would have the digital radar data and another would not (alternating role from case to case to eliminate individual skill as a factor). However, forecaster manpower was limited and low visibility cases are not that frequent (about 50/year), so we had to concentrate the effort on determining the combined benefit of network and radar digital data. Even if more forecasters were available, the "obvious" test would likely have been premature. When the mesonet forecast experiments began, the forecasters were quite unfamiliar with the new scale and frequency of reports, but the philosophy was that they would learn as the experiments progressed. Indeed, the results through two years of testing show improvement in the use of mesonet data as time went on. The forecasters were even less familiar with the use of weather radar in forecasting, and there were only about 20 radar cases a year, so the learning process would be expected to be much longer.

A brief study was made of cases involving precipitation, comparing the scores when radar was available against when it was not (equipment failure). When twelve cases of each condition were compared, the scores were nearly identical. However, the cases with radar were primarily during the first year, and those without radar were during the second year when the forecasters had grown more skillful. So, while at first glance the digital maps might appear to have been of no value, when the trend in skill is taken into consideration, the value of the radar would appear to increase.

4.3 Severe Weather Forecasts

During the past three summers, tests were made using the digital radar and mesonet maps to forecast convective weather conditions that cause disruption of activity and damage to airfields. The first year the tests were designed to determine how well the forecasters could time the arrival of the storm and predict its

intensity. Since we had few operating rain gauges, we based the timing on the occurrence of maximum extinction coefficient (minimum visibility) and predicted peak gust as well as maximum extinction coefficient. Forecasts were made for as many stations as the forecaster could handle, though he concentrated on those where the threat was the greatest, and forecasts were frequently updated, usually at ten-minute intervals. The results of this experiment proved very difficult to evaluate. Without experience or the benefit of radar-weather relations, the forecasters were over-predicting the severity of the storms and there were many cases of storms that either just missed stations or dissipated prior to arrival – the "false alarm" rate was quite high. With the few storms that did hit stations there were problems with multiple maxima in extinction coefficient – which one corresponded to the radar cell that was forecast to hit? Was a peak gust a half-hour later from the same storm or a different storm? Perhaps the most serious difficulty was that there really was not a single severe storm in the sample that would have caused wind damage at the network sites (one storm at one station had a peak gust of 19 mps).

The following two summers, the forecasts were made for the probability of low visibility (less than 800 m or 1/2 mile, daytime) strong gusts (over 14 mps) and heavy rain (greater than 15 mm or 0.6 in). The winds and rain could occur any time from 6 to 90 minutes after the forecast was made and the visibility probability was for each of six time periods of increasing duration, for example, 6 to 9 min, 10 to 15 min, ···, 61 to 90 min. (A sample forecast form is shown in Figure 8.) The variable duration allows for speed errors which produce greater timing errors at longer lead times. Again, forecasts were made for as many stations as possible and updated as often as every ten minutes. And, again there were very few thunderstorms for the tests. Early in July 1974, a violent lightning storm did roll into the network, but the forecasts halted when a power failure stopped the radar. Even worse, the forecasts could not be verified as the intense lightning knocked out communications to 70 percent of the network stations. Two weeks later a less violent storm struck, and even this one produced a five-minute computer halt due to power surge. Some 25 forecasts were made and verified and the results show a 26 percent skill score relative to climatology for extinction coefficients and 30 percent for wind gusts. A meaningful evaluation of the heavy rain probabilities cannot be made because the heavy rain condition was not observed.

In 1975, storms were watched closely on some ten afternoons, but no forecasts were made as the threats never appeared serious. On the night of 25 July a squall-line approaching from New York State was recorded on tape, and although the storms dissipated as they reached the network, there was a small tornado in Springfield, Mass., about midnight (EDT). The radar intensities around midnight

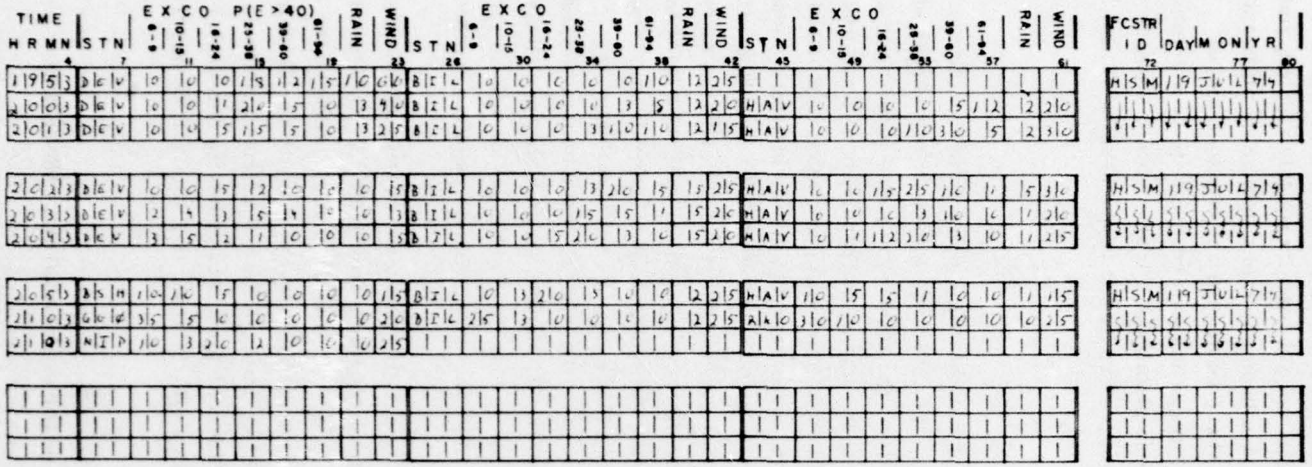

Directions for Severe Weather Forecast Form

1. For each of the six time periods beginning with current radar-map-time plus 6 minutes through time plus 9 minutes, forecast the probability of one-minute mean extinction coefficient greater than $40 \times 10^{-4} m^{-1}$. Note: Because of the uncertainty in speed, direction, and development, rarely is one justified in placing a probability greater than 60 percent in one of the forecast periods (there is no room for a 100 percent forecast).

2. For RAIN, enter the probability that more than 0.60 in. of rain will fall in the 90-minute period beginning with the current radar-map-time. (Extinction coefficient will be used for verification if rain gauge data are unavailable.)

3. For WIND, enter the probability that a peak gust greater than 27 knots will occur in the 90-minute period.

Figure 8. Sample Severe Weather Forecast

were about as high as ever seen in daytime and certainly most unusual for that time of night and that range. The case has not yet been thoroughly studied, but the echoes near Springfield do not seem to have been any more intense or different in pattern than those further to the north, where no severe activity took place.

Another attempt at severe weather forecasting will be made in the summer of 1976, and perhaps the storms will be more plentiful. We also hope for better radar performance as the FPS-77 was out for repairs in both August 1974 and August 1975.

4.4 Preliminary Conclusions

While there is little quantitative information at this point as to the value of digital radar in the forecast experiments, the forecasts left definite impressions in the minds of the forecasters. For utility, the hard-copy radar maps were a definite hit. The forecasters made much less use of the radar when it was available only on the scopes or even displayed on a micro-film projector (simulated real-time cases). A use that was not anticipated was the determination of mesoscale motion vectors from the radar which often provided useful in locating "upwind" mesonet stations to use as a forecast guide. There were really not many cases when the radar information was the primary reason for making a forecast of a major change in extinction coefficient, and most of these were in snow storms. We were not at all impressed with the idea that rain showers "wash out" fog beneath – indeed we had seen some cases when the arrival of the rain coincided with decreased visibility or no change at all. The effect of such showers likely depends on the drop-size distribution (which radar does not give) as well as turbulent wind motions and fog thickness. Certainly this problem requires further study.

One of the lasting impressions of the real-time forecast experiments is the vast quantities of weather information absorbed (often frantically) in the short time between 15-min forecasts. Indeed, the forecaster has 20 pages printed by the computer every 15 minutes, in addition to conventional data. Obviously an effort must be made to help the forecaster digest all this information. A simple system is to have the computer prepare objective "guidance" forecasts which the forecaster can use or not use as he sees fit. Preliminary efforts along this line will be described in Section 6.

5. RELATIONSHIPS BETWEEN RADAR SIGNAL RETURNS AND WEATHER PARAMETERS

To use the radar as a forecast aid, one must not only be able to locate and track the storm, but also determine the associated weather conditions. We would

expect intuitively that more intense precipitation will produce stronger radar returns. Indeed, researchers have found quantitatively useful relations between radar return and rainfall rate,[4] snowfall rate,[5] and hail occurrence.[6] In this section we shall briefly examine the theoretical basis for radar-weather relationships and present preliminary data from experiments using the radar and the mesonet observations.

5.1 Theoretical Basis for Radar-Weather Relationships

If the radar beam is uniformally filled with precipitation particles, at some distance "r," then the returned signal "P_r" can be expressed by

$$P_r = \frac{K}{r^2} C Z \quad , \tag{1}$$

where K is a function of the radar itself (including transmitted power, beam width, wave length, antenna gain, and receiver gain), C is a function of the precipitation type (index of refraction, shape, and orientation) and Z is the reflectivity factor defined by

$$Z \equiv \Sigma N_D D^6 \quad ,$$

with N_D being the number of particles of diameter D.

Thus, we can write

$$Z = \Sigma N_D D^6 = \frac{r^2 P_r}{K C} \quad . \tag{2}$$

The digital output of the DVI is a measure of $r^2 P_r$, the quantity C has been determined for different types of precipitation theoretically and experimentally, and the remaining factor K can be determined either through a calibration of the radar system, or through comparisons with rainfall rate. To develop and use radar-weather relationships, it is not so important to know the precise value of K, as to

---

4. Marshall, J.S., Langville, R.C., and Palmer, W. McK. (1946) Measurement of rainfall by radar, J. Meteor., 4:186-192.

5. Sekhon, R.S. and Srivastava, R.C. (1970) Snowsize spectra and radar reflectivity, J. Atmos. Sc., 27:299-307.

6. Donaldson, R.J., Chmela, A.C., and Shackford, C.R. (1960) Some behavior patterns of New England hailstorms. Physics of Precipitation, American Geophysical Union, Wash., D.C., 354-368.

know that it does not change with time. The subject will be discussed further in Section 7 on calibration.

The most thoroughly explored relation is that of radar and rainfall rate. While rainfall rate itself is not normally an important factor in airfield operations, it does provide a means for an approximate calibration for the radar. The rainfall rate can be expressed by

$$R = \Sigma \frac{\pi}{6} N_D D^3 f_D \quad . \qquad (3)$$

For drops in the size range of 1- to 4-mm diameter (those that contribute most to rainfall) the fall velocity f_D can be approximated[7] by $f_D = \alpha D^{1/2}$, where alpha is a constant of proportionality. Thus,

$$R = \frac{\pi\alpha}{6} N_D D^{7/2} \quad . \qquad (4)$$

The extinction coefficient E, which is directly related to visibility[8] can be related to drop size by

$$E = \frac{\pi}{2} \Sigma N_D D^2 \quad . \qquad (5)$$

One quickly notes that all of these parameters, Z, R, and E, are related to D, but with a different power. Without some knowledge of the size distributions of precipitation particles, it is difficult to proceed any further in relating these parameters. In 1948, Marshall and Palmer[9] undertook the difficult task of determining raindrop spectra, and from observations noted that the number can be related to size by $N_D = N_o \exp(-\Lambda D)$, a relation experimentally verified by others such as Ohtake[10] and Waldvogel.[11] Srivastava[12] has shown theoretical reasons why this exponential distribution should be observed below cloud level.

7. Weickmann, H.K. (1957) Physics of precipitation, Amer. Met. Soc. Meteorological Monographs, Vol. 3, No. 19, p. 228.
8. Middleton, W.E.K. (1952) Vision Through the Atmosphere, Toronto, University of Toronto Press.
9. Marshall, J.S. and Palmer, W. McK. (1948) The distribution of raindrops with size, J. Meteor., 5:165-166.
10. Ohtake, T. (1970) Factors affecting the size distribution of raindrops and snowflakes, J. Atmos. Sc., 27:804-813.
11. Waldvogel, A. (1974) The N_o jump of the raindrop spectra, J. Atmos. Sc. 31:1067-1078.
12. Srivastava, R.C. (1967) On the role of coalescence between raindrops in shaping their size distribution, J. Atmos. Sc., 24:287-292.

We can now convert the previous summations to integrals and substitute the exponential distribution of N_D. When we then integrate from zero to infinity* we now find

$$Z = \int N_D D^6 \, dD = N_o \int_o^\infty \exp(-\Lambda D) D^6 \, dD = \frac{6!}{\Lambda^7} N_o \quad . \tag{6}$$

$$R = \frac{\pi\alpha}{6} N_D D^{7/2} \, dD = \frac{\pi\alpha N_o}{6} \int_o^\infty \exp(-\Lambda D) D^{7/2} \, dD = \frac{\pi\alpha}{6} \frac{3!\sqrt{\pi} N_o}{\Lambda^{9/2}} \quad . \tag{7}$$

$$E = \frac{\pi}{2} \int N_D D^2 \, dD = \frac{\pi N_o}{2} \int_o^\infty \exp(-\Lambda D) D^2 \, dD = \frac{\pi}{2} \frac{2! N_o}{\Lambda^3} \quad . \tag{8}$$

A "typical" exponential distribution of drop sizes is shown in Figure 9. The associated rainfall rate of 5.7 mm/hr and extinction coefficient of 15×10^{-4} m^{-1} are values we often observe in moderate to heavy rain, when fog is not present.

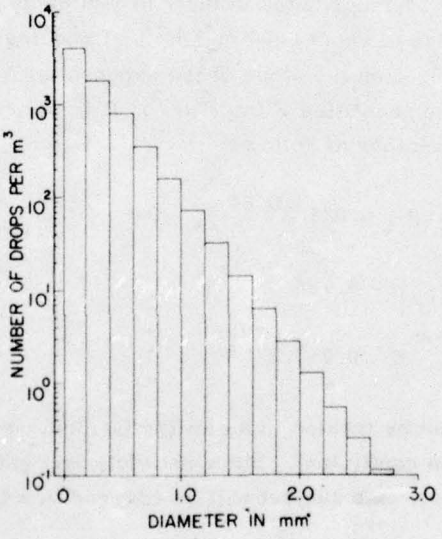

Figure 9. Raindrop Size Distribution for Moderate Rain

*To be physically more realistic, we should integrate only out to maximum drop size of about D = 6 mm, and the answer can be found in a table of incomplete gamma functions.

In Table 1 we see the relative contributions of three different drop-size categories to the parameters Z, R, and E. Clearly the smallest drops contribute little to the radar return, but are very important to visibility, and moderately important to rainfall rate. The largest drops are only important to the radar return, as their numbers are simply too small to be important to rainfall rate or extinction coefficient.

Table 1. Relative Contribution of Different Drop Sizes to Radar Reflectivity, Rainfall Rate and Extinction Coefficient, Based on Distribution in Figure 7

Drop size	Z	R	E
0 to 1 mm	0.12	0.47	0.77
1 to 2 mm	0.58	0.46	0.22
2 to 5 mm	0.30	0.07	0.01
Total	1.00	1.00	1.00

Marshall and Palmer[9] further noted in their experiments that N_o was essentially constant, with a value of about 8000 $m^{-3}m^{-1}$. Choosing a reasonable value of α of 460 cm $S^{-1}mm^{-1/2}$, then the slope of the exponential Λ can be related to R by $\Lambda = 4.3\ R^{-0.22}$. The quantities Z (mm^6m^{-3}), R (mm hr^{-1}), and E ($10^{-4}m^{-1}$), can all be related to one another as follows:

$$Z = 200\ R^{1.56} \quad \text{or} \quad R = 0.033\ Z^{0.64}\ , \tag{9}$$

$$E = 3.07\ R^{0.67} \quad \text{or} \quad R = 0.186\ E^{1.50}\ , \tag{10}$$

$$Z = 14.6\ E^{2.33} \quad \text{or} \quad E = 0.317\ Z^{0.43}\ . \tag{11}$$

Snowfall rate can also be treated in a similar fashion, and be related to radar reflectivity and extinction coefficient. Since snowfall data gathered in the mesonet have not yet been analyzed, this subject will be covered in a later report.

5.2 Empirically Derived Radar-Weather Relationships

At the time the first maps from the program RADAR I became available, work was begun collecting data to develop radar-weather relations. The basic Z-R relation is known to be reasonably valid, but we did need to collect simultaneous rainfall and radar data to establish a system calibration, since previous attempts at absolute calibration had not been successful. The Z-E and E-R relations had not been well explored, largely because until the Forward Scatter Visibility Meter was developed[13] there was not an instrument available to measure extinction coefficient over a sufficiently wide range.

5.2.1 RADAR RETURN VERSUS RAINFALL RATE

In order to obtain data on rainfall rate, we had obtained some ten tipping bucket rain gauges, which were then placed at many of the automatic mesonet stations. The gauges were designed to count the number of tips, one for each 1/100 in. (0.39 mm), and convert the count to a 0 to 5 VDC signal to be compatible with other sensors. By interrogating the station every 10 seconds, it is possible to calculate the time of each tip to within 5 seconds, if we assume that the tip occurred 5 seconds before interrogation. If the tips are one minute apart (R = 15 mm/hr) the rainfall rate should be accurate to ±10 percent, and if three minutes apart (R = 5 mm/hr) accurate to ±5 percent. While the principle is quite simple, it took almost two years before we were consistently receiving reliable rain-gauge data (during the first year, primary attention was paid to other sensors). Even now, periodic attention (monthly) is necessary to remove debris from rain-gauge funnels and ensure proper tipping. Winter-time operation is quite difficult as the heat applied to melt snow and ice may evaporate some precipitation before it is measured, particularly if the heating is strong enough to melt heavy snowfall rates.

A comparison of 3-min rainfall rates with averaged radar return is shown in Figure 10. The data shown were obtained from station BIL located 10 km north of the radar, during four heavy rain storms several months apart. The rainfall rate was obtained by assuming the bucket filled linearly with time before tipping. The sloping line represents the previously derived relation $Z = 200\ R^{1.56}$, and the overall fit of the data can be considered to be good. The scatter is quite large, but is typical of what other investigators have found. Marshall and Gordon[14] once remarked "The goodness of the correlation is the subject of continuing debate. The scatter shown --- is typical and seems to be just enough to permit its use by

---

13. Muench, H.S., Moroz, E.Y., and Jacobs, L.P. (1974) Development and calibration of the forward scatter visibility meter, AFCRL-TR-74-0145, Instrumentation Paper No. 217.

14. Marshall, J.S. and Gordon, W.E. (1957) Radiometeorology, Amer. Meteor. Soc., Meteorological Monographs, Vol. 3, No. 14, p. 96.

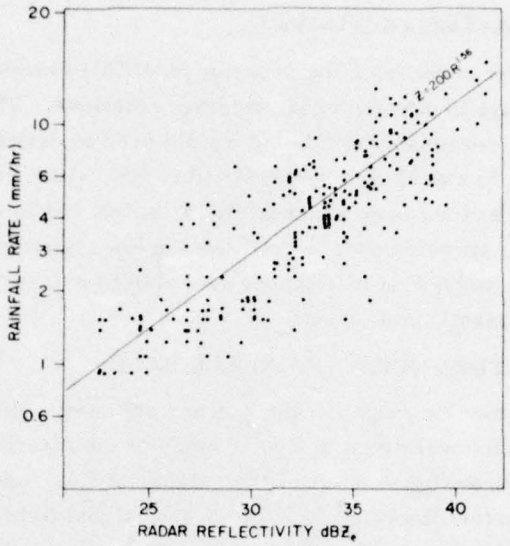

Figure 10. Correlation of Rainfall Rate to Radar Return for Mesonet Station BIL

by some authors as evidence that you can measure rainfall by radar, by other authors as evidence that you cannot."

A variety of factors contributes to the scatter of the points in Figure 10. If there is a long time between tips, such as the more than five minutes for rainfall rates of 3 mm/hr and less, then the assumption of linear fill rate may lead to serious error. The relative radar calibration has been made through ground echo comparisons and this procedure is probably no more accurate than ±1 dB. Drift of the radar calibration during the storm and the round-off of the archived data to 3-dB steps would also contribute an uncertainty of ±1 dB. Thus, the uncertainty in Z would be about ±40 percent and would mean errors in specifying R of about ±25 percent, but this is much smaller than the error of specification represented by the points in Figure 10. However, investigators such as Waldvogel[11] have found that N_o is not a constant, as was assumed by Marshall and Palmer,[9] and that large, systematic variations in N_o take place over periods of minutes to hours, apparently related to basic precipitation processes. While the basic Z-R relation is valid in general, it does not necessarily apply at a particular time and place.

For forecast purposes, the scatter indicates what the limiting accuracy would be, assuming the radar pattern could be perfectly predicted. From these four storms with widespread rain, the rms error of specifying ln R is about ±0.6, which would mean specifying R to an accuracy of about ±60 percent, for all stations

combined. To achieve the same accuracy in specifying rainfall rate by using rain-gauges instead of radar, we would need a network of stations about 40 km apart. Rainfall forecasts from "perfect" radar forecasts would be about as accurate as persistence forecasts out at fifteen minutes, indicating the greatest value for radar would be in the period beyond fifteen minutes. These statistics are based only on four storms, individually similar, but the statistics for convective showers would likely be somewhat different.

5.2.2 RADAR RETURN VERSUS EXTINCTION COEFFICIENT IN RAIN

A considerable effort was made to gather data for radar-extinction coefficient relations, for use in real-time forecast experiments. Two informal reports were prepared as forecast guides during the first year of operations. Since then, large numbers of comparisons have been obtained, especially after digital radar maps were archived on magnetic tape. In assembling these data, one must be careful to exclude episodes of fog, from the rain cases, as fog has a drastically different drop-size distribution. This separation is not always easy, but we did find that in cases of rain with cloud base at least 200 m above, that the extinction coefficients from the 15- and 30-m levels on the tower behaved nearly identically, which was not at all the case in fog. Also, if fog is present in a rain storm, the hilltop stations, such as Boston Hill and Sagamore Hill, will show very high extinction coefficient, often equivalent of 1/4 mile or 400-m visibility or less, and these extinction coefficients are too persistent to be due to rain.

Comparisons of extinction coefficients and radar return for four rain cases are shown in Figure 11. The linear relation shown in the figure, $E = 0.63\ Z_e^{0.4}$, has the same exponent as derived in Eq. (10), but the coefficient, 0.63, is considerably greater, indicating that the extinction coefficients are larger (by 80 percent) than would be expected from Marshall-Palmer drop-size distributions.

Some of our early studies of heavy rain showers indicated that the maximum extinction coefficient usually occurred a couple of minutes after the maximum radar return from above the station. To investigate this phenomenon further, correlation coefficients were computed for different time lags between the radar return and the extinction coefficient, using data from the first three storms. Results from some of the stations are shown in Figure 12. Quite clearly there is a 1- to 3-min lag, and the positive sign indicates the radar maximum occurred earlier. Similar lags were also seen in comparisons of radar and rainfall rate, but there were fewer data. When data were assembled for Figures 10 and 11, a two minute shift was made to partially compensate for the lag. In Figure 12, the distance from the radar to the station is shown in parentheses to the right of station identification code. If the lag were simply due to the time it took the particles to fall from the radar beam (at one degree elevation angle) to the forward scatter

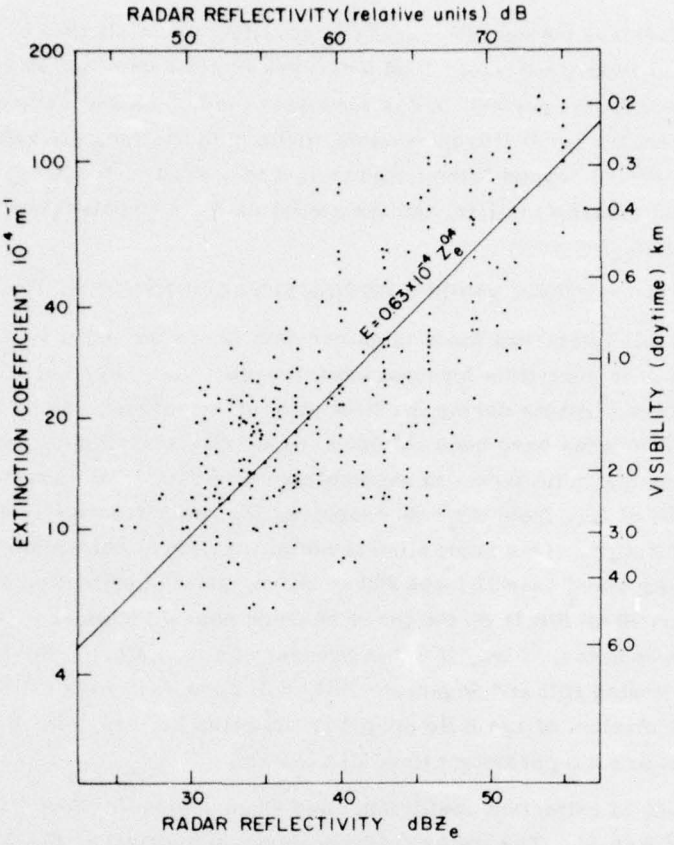

Figure 11. Correlation of Extinction Coefficient to Radar Return for Mesonet Station BIL

visibility meter, then stations further out should have a longer lag. However, from these data, there does not seem to be a direct relation between lag and distance. On the other hand, one does note that the best correlation coefficients do occur closest to the radar and the worst ones furthest out. This decay of correlation coefficient with distance may be due to a problem of the radar beam being less uniformly filled with drops at large distances, or, perhaps due to horizontal drift of the drops between the time they leave the beam and reach the visibility meter. Wilson and Pollock[15] found the accuracy of rainfall specification, using radar, decreased with increasing distance.

15. Wilson, J.W. and Pollock, D.M. (1974) Rainfall measurements during hurricane Agnes by three overlapping radar, J. Appl. Met., 13:835-844.

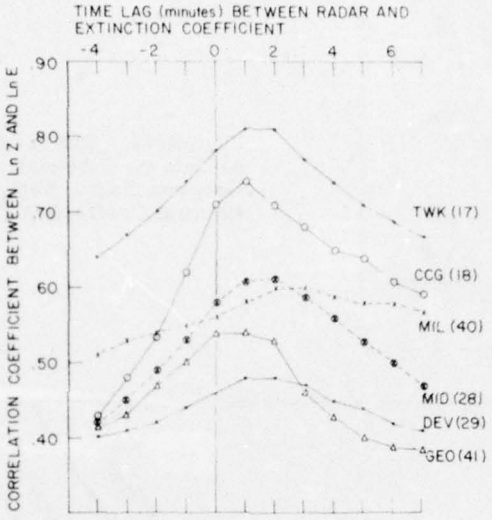

Figure 12. Correlation Between Radar Return and Extinction Coefficient for Different Time Lags

Next, the question of time averaging was examined. Correlation coefficients of radar return versus both extinction coefficient and rainfall rate were computed for time averages of one, three, five, seven, ten, and fifteen minutes. The plots in Figure 13 (based on all stations combined) show that the correlation coefficient improves as one uses longer and longer time averages, although the amount of improvement for periods longer than five minutes is not great. Apparently, the shorter period fluctuations in visibility and rainfall are not as well correlated to radar return as are the longer period ones, though a physical reason for this is not obvious.

5.2.3 RAINFALL RATE VERSUS EXTINCTION COEFFICIENT

There would seem to be little point in determining a relation between rainfall rate and extinction coefficient if we are primarily concerned with applying radar information to the short-range forecast problem. However, as shall be seen, there is a diagnostic value to this exercise. From the four cases of widespread rain, 3-min mean values of rainfall rate and extinction coefficient were extracted and are shown plotted in Figure 14. The upper sloping line is that which would be expected from Eq. (11) based on the Marshall-Palmer drop-size distribution. Clearly this differs significantly from the "best fit" line shown. As in the radar versus extinction coefficient, the exponent in the relation is as expected, but the

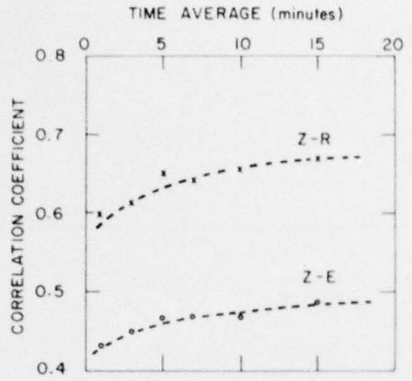

Figure 13. Effect of Time-Averaging of Data on Correlation Coefficients Between Radar Return (Z-R) and Extinction Coefficient (Z-E)

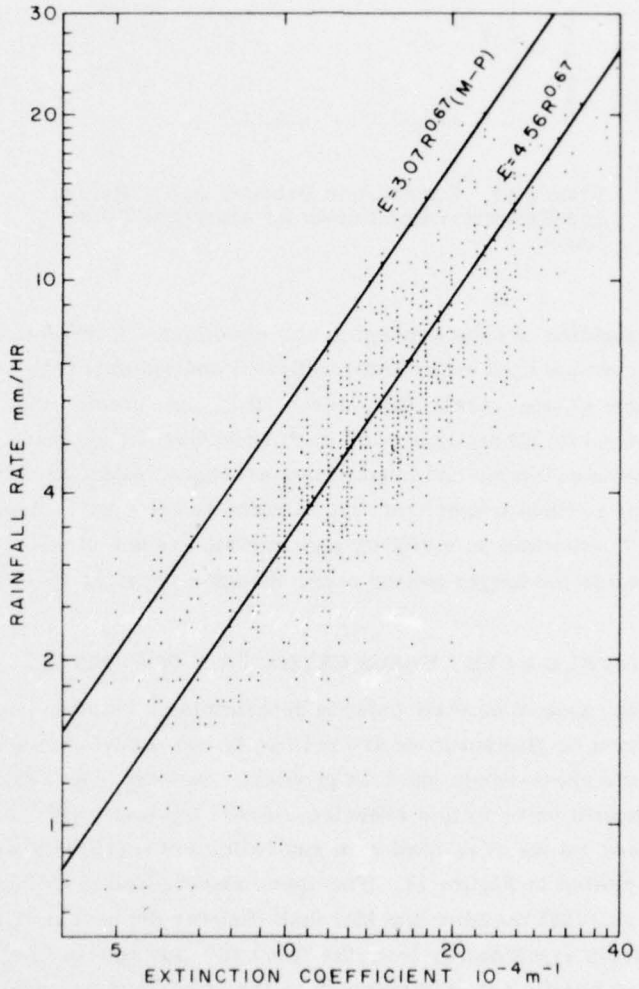

Figure 14. Correlation of Extinction Coefficient to Rainfall Rate

coefficient indicates extinction coefficients are about 50 percent greater. With the rainfall rate versus extinction coefficient, there could be some confidence in the calibration of both forward scatter visibility meters and rain gauges. The visibility meters were carefully checked against transmissometers in fog[13] and in snow (unpublished report) and the absolute calibration is within 10 percent. There have been problems with the performance of the transmissometers in the mesonet during heavy rain (likely, droplets splashing onto optics) precluding valid comparisons, so we cannot yet completely rule out the possibility that there is an unexpected effect of rain on the visibility meter. The rain data from the tipping bucket gauges are periodically checked against weighing-bucket data and the differences rarely exceed 10 percent.

A more plausible explanation is that the Marshall-Palmer drop-size distribution formulation is simply not valid for small drops. We can speculate that there is an unexpectedly large number of drops too small to affect the rain gauges or radar reflectivity. Since we do find good correlations (0.6 to 0.9) between rainfall rate and extinction coefficient, the increases and decreases in the numbers of these small drops must occur simultaneously with corresponding changes in the numbers of larger drops that affect rainfall rate (and radar return). We might be seeing showers of drizzle-sized droplets (about 0.3 mm) occurring as part of the same vertical motion pattern that is producing the showers of larger droplets. Or, perhaps there are large numbers of fog-sized droplets (less than 0.1 mm) formed in the wakes of the large-size rain drops. Certainly further confirmation of this difficulty with the Marshall-Palmer distribution is desirable, which should be forthcoming from an AFGL project underway at Otis Air Force Base. A rigorous investigation, however, would require special equipment to measure drop sizes over a very wide range, during rain storms.

6. DEVELOPMENT OF OBJECTIVE FORECAST AIDS

The real-time forecast experiments impressed upon the forecasters the desirability of having objective forecast aids available to reduce the problem of coping with an enormous data base in a short time. There are three basic routines that the subjective forecaster follows: first the tracking of significant radar patterns to determine a motion vector; second, forecasting the radar values (by extrapolation) that will occur at each station as a function of time; and third, the conversion of forecast radar values to weather parameters. This section will describe the work that has been done on each of these three routines, followed by an example of application to a severe weather forecast.

6.1 Objective Determination of Radar Echo Motion Vectors

In the manual determination of a motion vector, the radar meteorologist periodically marks the time and position of significant features of radar patterns (usually on the PPI scope). These features might be center-of-gravity (in the case of an isolated echo) or perhaps a line connecting a series of cells, or perhaps a center of maximum intensity found by gain reduction.

From a series of two or more positions, the meteorologist determines a direction and speed. If there were but a single rainstorm (or snowstorm) entirely within the grid of the digital radar data, the task of tracking by computer would be relatively simple. For example, one could compute the position of the center of mass by averaging the X-coordinates of all the non-zero radar values and also the Y-coordinates. Thus

$$x = \frac{1}{n}\sum_{i=1}^{n} x_i \quad ; \quad y = \frac{1}{n}\sum_{i=1}^{n} y_i \quad .$$

From maps at different times, t_1 and t_2, one computes the average u and v components of motion by

$$u = \frac{\bar{x}_2 - \bar{x}_1}{t_2 - t_1} \quad ; \quad v = \frac{\bar{y}_2 - \bar{y}_1}{t_2 - t_1} \quad .$$

Since x_i and y_i are just integers representing the row or column number the resolution of x and y improves as n gets larger. For a given resolution or accuracy in the position data, the accuracy of u and v increases if the time increment $t_1 - t_2$ is made larger. Thus, we would like to work with large radar echoes, and use long time intervals.

Unfortunately, we typically find many storms on the digital maps, and not just one, some moving with different speed and direction than others. Also, at any given time some may be moving onto the map area and others leaving, and some may develop within the map and others disappear. Added to these complications, we have a "ground clutter" pattern due to echoes from hills and towers, that does not move but may oscillate in intensity. Blackmer, et al[16] tackled this problem through a procedure that merges values above a certain threshold (about 40 dB Z_e) to form echo "clusters." They then match clusters at successive times and use a

16. Blackmer, G.L., Duda, R.O., and Rebah, R. (1973) Application of Pattern Recognition Techniques for Digitized Radar, Final Report, Contract 1-36072, Stanford Res. Inst., Menlo Park, Calif.

cross-correlation technique to determine the X and Y displacement that produces the best correlation. Each cluster is treated independently and previous motion vectors are used as a first guess in the matching process. Special logic is used to treat newly developed and disappearing cells, and ground-clutter problems are avoided by ignoring data within a 35 km radius of the radar. Austen and Bellon[17] have also used a technique that involves cross-correlation. They first match echo pairs from successive maps, then make a first guess motion by computing the displacement of the center of mass, and then compute a more precise displacement by maximizing the cross-correlation.

One objective of our project was to develop techniques that could be used in real-time on the HW DDP 324. While the techniques of Blackmer, et al[16] and Austen and Bellon[17] have been well tested, the FORTRAN listing for the former indicated larger core requirement than is available on our computer. Thus we turned to developing an alternate technique. The first thoughts were to try simple procedures and introduce modifications as problems arose. Tracking echo edges became the starting point. Figure 15 illustrates the procedure for identifying leading and trailing edge for a particular pattern. Radar intensities from three adjacent rows have first been averaged to produce the values one sees, and the edges are identified as the positions of the non-zero values furthest to the left and to the right.

Tracking the two edges will provide information on the larger scale motions. But it would also be desirable to have information on the motion of smaller patterns contained within the edges. A straightforward technique is to make a harmonic analysis of the pattern between the edges and store the phase angles of significant amplitudes. Amplitudes and phase angles would normally be computed from the following formulation

$$A_n = \frac{2}{I} \sum_{i=1}^{I} R_i \sin \left[\frac{2\pi ni}{I} \right] ,$$

$$B_n = \frac{2}{I} \sum_{i=1}^{I} R_i \cos \left[\frac{2\pi ni}{I} \right] ,$$

17. Austin, G. L. and Bellon, A. (1974) The use of digital weather radar records for short-term precipitation forecasting, Quart. J. Roy. Met. Soc., 100:658-664.

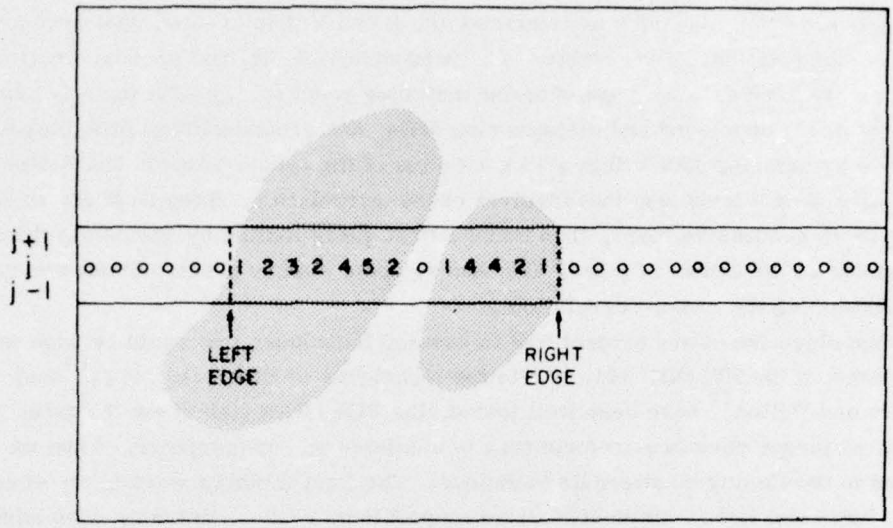

Figure 15. Technique for Deriving Position Parameters

$$C_n = \left[A_n^2 + B_n^2\right]^{1/2} ,$$

$$\Phi_n = \frac{I}{2\pi m} \arctan \left[\frac{A_n}{B_n}\right] ;$$

A_n and B_n are two components of wave number n in the interval I = 1, I, with net amplitude C_n and position of peak amplitude at Φ_n; R_i is the radar amplitude. The program requires that I be at least as large as 3, and harmonics are only computed for wave numbers up to and including I/3. With some waves based on a small number of points, more representative A_n and B_n values are obtained if one uses integrated values of sine and cosine as follows

$$A_n = \frac{2}{I} \sum_{i=1}^{I} R_i \int_{i-1/2}^{i+1/2} \sin\left[\frac{2\pi n i}{I}\right] di$$

$$= \frac{1}{\pi n} \sum_{i=1}^{I} R_i \left\{ \cos\left[\frac{2\pi n}{I}(i - 1/2)\right] - \cos\left[\frac{2\pi n}{I}(i + 1/2)\right] \right\} ,$$

$$B_n = \frac{2}{I}\sum_{i=1}^{I} R_i \int_{i-1/2}^{i+1/2} \cos\left[\frac{2\pi mi}{I}\right] di$$

$$= \frac{1}{\pi m}\sum_{i=1}^{I} R_i \left\{\sin\left[\frac{2\pi m}{I}(i + 1/2)\right] - \sin\left[\frac{2\pi m}{I}(i - 1/2)\right]\right\} .$$

(While the introduction of sine and cosine functions into this problem might seem like an undesirable complication, the basic radar program already contains sine and cosine tables for use in the coordinate conversion routine.)

This analysis provides the locations of edges and peaks in harmonics, which when matched with corresponding locations at a later time will yield displacement vectors. Previously, we noted that more reliable vectors are obtained by using longer time increments, but, if one waits very long, echoes appear and disappear and slide from one row or column to the next. An interesting solution is to use very short time intervals, one or two minutes, and simply disregard displacements that indicate speeds greater than 40 mps. These discarded values would be caused by displacements of 4 grid increments or more and would likely be due to cell development or decay, and not real motion. This procedure was tested on a fast-moving (non-severe) shower system and a 2-min time interval was found adequate for the 1-km maps. The components did contain some undesirable short period fluctuations, but these can be largely removed by taking 5-min averages. During these tests, the weakest harmonics were found to have poor coherence, so, harmonics with amplitude less than 1.5 dB are ignored. Also, to focus attention on the stronger echoes and those with short wavelength, and therefore strong horizontal gradient, the following weighting function was formulated

$$W_n = (C_{n1} + C_{n2} - 3\ \text{dB})^{1/2} \left(\frac{n}{I}\right)^{1/4} .$$

For the weighting function of the edge displacement, the amplitude of the zeroth harmonic is used, with the constant 0.22 in place of the factor $(n/I)^{1/4}$.

In using the fine-scale maps, the problem of ground clutter becomes very important, as we cannot afford to simply ignore all data within the range of the farthest ground return. During fair weather we have noted high stability in the return from the ground return, presenting a possibility that it might be mathematically removed from the maps. Since the radar value is the logarithm of the signal, we cannot simply subtract out the fair weather value at each grid point. On the

other hand, with values as coarse as the 3-dB steps used here, it is not necessary to convert back to Z value, subtract and re-convert to dBZ. Instead, if the grid value is equal to or less than the normal ground clutter value, a no echo value is assumed. If the value is 3 dB higher, then 3 dB is subtracted. If the value is 6 dB or more greater, no change is made. This procedure is quite effective in removing the ground returns from the hills beyond 8 km, but leaves a scintillating pattern closer to the radar. Fortunately, this residual pattern is rather spotty and disorganized, and appears to have little effect on the motion vector routine.

This motion vector routine was programmed in FORTRAN and checked out on the AFGL CDC 6600, using a storm case from May 1974. It was during this checkout procedure that the 2-min interval was chosen and the weighting formulated. The first independent test of the program was a squall line of 19 July 1974. Computed west and south components of motion are shown in Figure 16, including individual values for every minute and the 5-min mean as well. About 2050 GMT a large storm was moving off the right edge of the grid, and the operator shifted the origin of the grid to continue to follow this storm, which accounts for the short gap in data at that time. The storm itself hit Hanscom AFB at 2105 GMT and lightning strikes disrupted the computer-radar system for several minutes.

The motion vectors from this routine are for use in simple extrapolation forecasts, and it is important that they be stable throughout the forecast period. As seen in Figure 16, the components obtained from single pairs of maps contain some unwanted high frequency fluctuations that are fairly well smoothed out by taking 5-min means. The vectors based on single pairs of maps differed from the 3-hr vector mean by ±24 percent, while the 5-min means differed by ±17 percent and 10-min means by ±14 percent. Obviously the longer the averaging time the more stable the vector, but waiting 10 minutes or more before making a forecast may not be practical when echoes first appear. Austin and Bellon[17] noted that spatial errors in forecasting individual echo displacement were about ±18 percent. Had we similarly forecasted and verified individual cell motions using the 10-min motion vectors, the errors would have been larger than the ±14 percent departure from the mean, as individual cells often move differently than the average over the whole grid, and so the techniques are probably very similar in accuracy.

6.2 Objective Forecasts of Radar Intensity

Given the speed S and the direction D from which radar echoes are moving, the task of predicting radar value as a function of time at a given point is relatively simple. One starts at the forecast location, using the latest digital radar map, and looks in the direction D a distance $S\Delta t$ to find the radar intensity that will arrive at Δt later. There are but two small worries. First, the echoes may

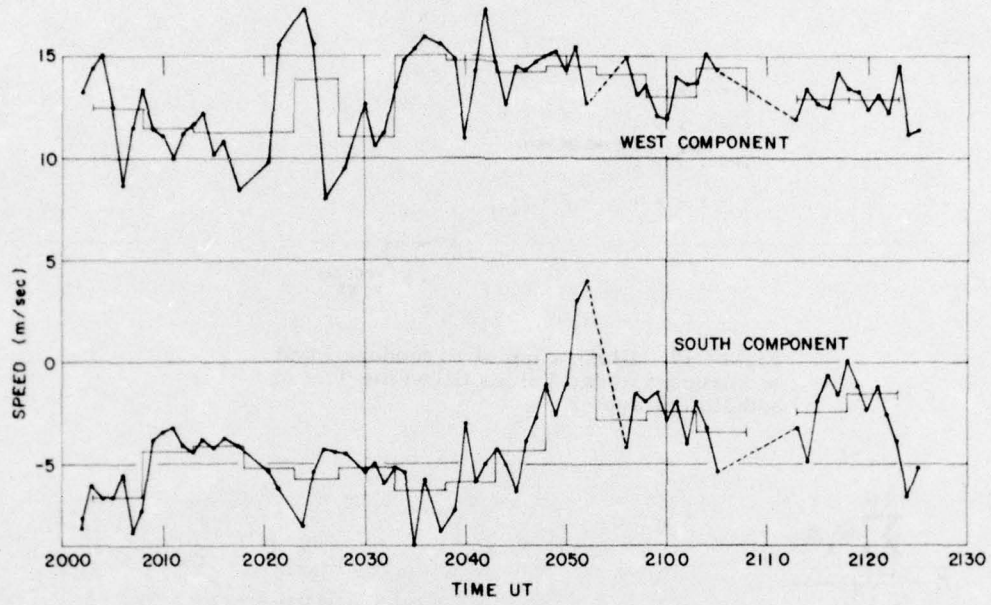

Figure 16. Instantaneous and Five-Minute Mean Objectively Determined Motion Vectors

develop or decay during the time period leading to a poor forecast, and second, the echoes may move in a direction different than the overall motion. The question of development is a difficult one and will be treated later when more cases have been collected to serve as a basis for new techniques. For the present we will assume translation without change in intensity. Compensation for uncertainty in the motion vector can be made by examining the radar values at points surrounding the point that will arrive at the forecast station Δt later. A procedure for this compensation looks at a 4-row by 6-column array surrounding the upstream point, as shown in Figure 17, and weights the radar value by the following factor

$$W = \exp\left[\frac{-3000\ r^2}{(S\Delta t)^2} + 1000\right] \quad ,$$

where r is in km, S in mps, and Δt in minutes. This formulation gives the outermost points of the array the least weight, but the relative contribution increases as the forecast time increases, consistent with a ±15 percent to ±20 percent uncertainty in the motion vector. To compute the weighted mean forecast value Z and standard deviation σ_Z, we use

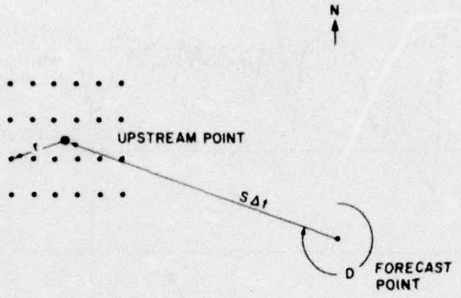

Figure 17. Illustration of Procedure Used to Forecast Radar Values Given the Time and Motion Vector

$$\bar{Z} = \frac{\sum_{i=1}^{16} W_i Z_i}{\sum_{i=1}^{16} W_i} ,$$

$$\sigma = \left[\frac{\sum_{i=1}^{16} W_i Z_i^2}{\sum_{i=1}^{16} W_i} - \bar{Z}^2 \right]^{1/2} .$$

The forecast program that was developed moves out at 1-min steps for 90 minutes,* or until the edge of the map is reached, computing $\bar{Z}$ at each step. Samples of three such forecasts prepared from the 2038 GMT radar map are shown in Figure 18, along with the radar values that were later observed. These are typical of what we find in that some fairly impressive forecasts can be made for dramatic changes in the 2- to 20-min forecast period, while forecasts for longer periods are more apt to show the effects of echo development or decay.

*In the forecasts verified in Section 6.4 only, a 60-min period was used to avoid inconsistency when some steps would have passed the edge.

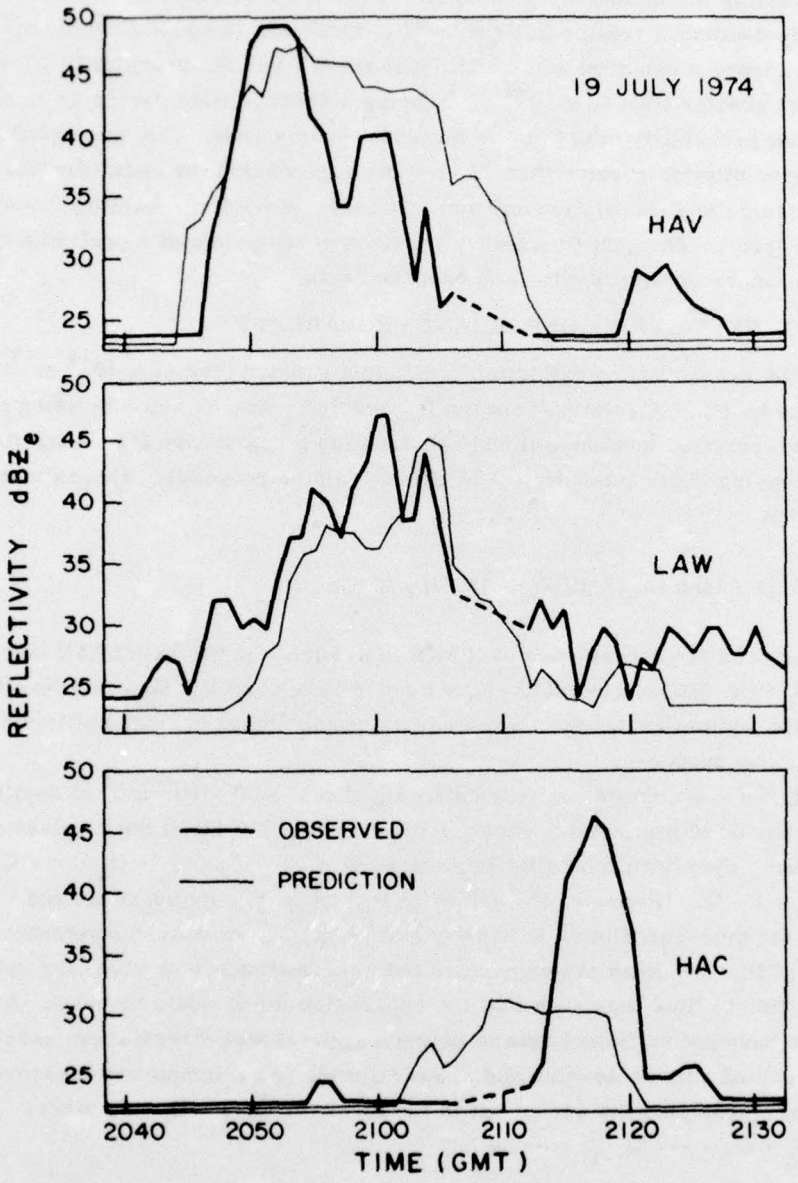

Figure 18. Sample of Three Forecasts of Radar Intensity, Using Objective Forecast Procedure

6.3 Forecasting Meteorological Parameters

Converting the minute-by-minute forecasts of radar intensity produced by the previously described routine into probability forecasts compatible with those shown in Figure 8 requires some additional work. For the probability of extinction coefficient greater than 40×10^{-4} m^{-1} during a specific time period we must compute a joint probability based on the forecast radar values. For the probability of 90-min precipitation greater than 15 mm, we can convert the radar forecasts to rainfall using the Z-R relation and sum, and then compute probability based on probable error. The gust probability required development of a preliminary routine based more on intuition than on recorded data.

6.3.1 EXTINCTION COEFFICIENT PROBABILITY

Let the probability of extinction coefficient greater than 40×10^{-4} m^{-1} at a given time be P_E. A relation between P_E and dBZ_e was obtained by using data similar to that used in Figure 11 and constructing a cumulative frequency diagram with increasing radar intensity. The curve could be reasonably approximated by the function

$$P_E = \{1 + \tanh [0.13\ (dBZ_e - 45.5)]\}\ /2 \quad ,$$

which was used for convenience as TANH is available in the FORTRAN compiler of the AFGL CDC 6600. Alternatively, we could have used a probability function polynomial approximation or even a table of values to obtain P_E with sufficient precision for our purposes.

Next, we must obtain the probability P_E that $E > 40 \times 10^{-4} m^{-1}$ at anytime during a period of n minutes. First, let $Q \equiv 1 - P_E$. If all of the n values are independent, the joint probability is given by $\hat{Q} = Q_1 \cdot Q_2 \cdot Q_3 \cdot Q_4 \cdot \cdots Q_n$. Thus $\hat{P}_E = 1 - \hat{Q}$. However, the values of P_E only a minute apart are not independent, as the auto-correlation is usually quite high. If we knew the auto-correlation function of P_E, we could either remove the interdependence or else take values of P_E at sufficient time lags such that the expression for $\hat{Q}$ would be valid. At this point, we have not sufficient data to define a general auto-correlation, much less one that varied with scale-size and shower speed. As a temporary measure, instead of multiplying the series out in the form $\cdots \hat{Q}_{i-1} \cdot Q_i \cdots$, where $\hat{Q}_{i-1} = Q_1 \cdot Q_2 \cdot \cdots Q_{i-1}$, we use

$$Q_{i-1} \cdot \left[1 - |\hat{Q}_{i-1} - Q_i|^{1/2} (1 - Q_i)\right] \quad .$$

This procedure effectively includes additional values only if they differ from others, and thus reduces the effect of auto-correlation. As more data are collected, a

more rigorous expression will be sought. We must also check to see if a probability based on the maximum radar intensity forecast for the period might be sufficiently accurate.

6.3.2 RAINFALL PROBABILITY

A 1-min rainfall can be obtained by applying the Z-R relation to the 1-min forecasts of radar intensity, which expressed in dBZ_e is

$$R = \exp [(dBZ_e - 51)/6.8] \quad .$$

The predicted 1-min values are then summed over 90 minutes to obtain a forecast of total rainfall. For rainfalls of more than a few millimeters an hour, the errors in predicting rainfall will be proportional to the rainfall. If R_o is the observed rainfall and R_f is the forecast, we would expect $[\ln R_o - \ln R_f]$ to be normally distributed. To compute the probability that the observed rainfall is greater than some threshold R_T, we again need a cumulative frequency function. Applying the tanh approximation we have

$$P(R_o < R_T) \simeq \left[1 - \tanh\left(\frac{\alpha}{2} (\ln R_f - \ln R_T)\right)\right]/2 \quad .$$

Introducing the exponential relation for tanh, this reduced to

$$P(R_o > R_T) = \frac{R_f^\alpha}{R_f^\alpha + R_T^\alpha} \quad .$$

With α set of 3, the distribution would correspond to forecasting with an error of ±50 percent. The uncertainty in converting radar measurements to rainfall, as indicated by the scatter in Figure 10, is about ±50 percent and the error in forecasting the radar value must also be added. On the other hand, the integration over 90 minutes will reduce the errors somewhat, and the figure of ±50 percent would be a reasonable first approximation.

6.3.3 GUST PROBABILITY

With very little data for guidance, a simple routine for maximum gust was formulated. Physically, thunderstorm gusts appear to occur when air aloft with high water content (rain, snow, and hail) descends, cooling by evaporation and melting, and spreads out upon reaching the ground. The horizontal accelerations that result in gusts are a result of density gradients, primarily due to temperature gradients. Since the downdrafts often reach the ground with a temperature near

the ambient dewpoint, the gusts should be related to the ambient dewpoint spread. In addition we would expect the gusts to be related to radar intensity as an indicator of the mass of precipitation that descended, and also to echo speed, as the downdraft should maintain some momentum of the winds aloft that is reflected in the echo speed. Combining these thoughts, the following relation for peak gust G_p was formulated

$$G_p = (20 + S)(3 + T - T_d)(dBZ_e - 25)/800 \quad ,$$

where the storm motion S is in mps, the ambient dewpoint spread $T - T_d$ is in Celsius and the r maximum radar value is in dBZ_e. The relation to dBZ_e is largely based on two storms that affected mesonet stations early in 1973.

To obtain the probability that the gusts will exceed a given threshold G_T at a network station, we assume the model is accurate to ±33 percent and following the same procedure for rainfall probability we find

$$P(G_p > G_T) = \frac{G_p^5}{G_p^5 + G_T^5} \quad .$$

6.4 Test of Objective Forecast Aids

The previously described routines were designed to make probability forecasts identical in form to those made by the real-time severe weather forecaster, as described in Section 4.3. The routines were run using data from the squall-line case of 19 July 1974, and comparisons were made with three types of forecast – the real-time or subjective forecasts, the objective forecasts, and climatological forecasts. For each forecast a "P" score was computed, defined by:

$$P = \frac{1}{n}\sum_{i=1}^{n}(P_f - P_o)_i^2 \quad ,$$

where P_f is the probability forecast and P_o is the observed probability (0.0 if the condition did not occur and 1.0 if the condition did occur). A skill score representing improvement over climatology was also computed. The resulting verifications for the three types of forecasts are shown in Table 2, based only on times and stations for which subjective forecasts were available.

Table 2. Comparison of Subjective, Objective, and Climatological Severe Weather Forecasts

	Extinction Coefficient			Gusts		
	n	P	skill	n	P	skill
Subjective	84	0.127	+0.26	17	0.327	+0.30
Objective	84	0.131	+0.24	17	0.327	+0.30
Climatology	84	0.7 0.172	±0.00	17	0.470	±0.00

Clearly, skill over climatological forecasts is demonstrated by both objective and subjective forecasts, although the level of skill is not very high. Also, we can be encouraged to see that the computer-based objective forecasts were similar in accuracy to the real-time forecaster. In all likelihood, if the real-time forecaster had the objective forecasts and motion vectors for guidance, he would have obtained yet higher skill scores.

The performance of the objective technique for all stations and all times on 19 July 1974 are presented in Table 3. There is a modest improvement over climatology for all time periods out to 60 minutes, though beyond 25 minutes the improvement is quite small. As before, the P score for the objective forecasts is better than climatology. Overall, the P-scores in Table 3 are lower than in Table 2 (which is a sub-set), a result of the real-time forecaster having chosen the times and places of greatest storm threat.

Table 3. Objective and Climatology Forecast Scores for all Forecasts

	Extinction Coefficient					Gusts
	Time Period (min)					
	6-9	10-15	16-24	25-38	39-64	6-64
number	400	400	400	385	385	383
P Objective	0.033	0.038	0.056	0.087	0.119	0.252
P Climatology	0.037	0.049	0.073	0.095	0.129	0.285
Skill-Objective	+0.11	+0.22	+0.23	+0.08	+0.08	+0.15

7. RADAR CALIBRATION

If the radar is to be useful as a forecast tool, the signal intensity and the position information must be reliable. The signal calibration errors must be kept small compared with the uncertainty in relating radar signals to weather parameters. In general, if the signal calibration is accurate to ±2 dB, then the variance due to signal error will be about 10 percent of the specification error. The position information errors must be kept small compared with the scale size of the echoes. Important precipitation patterns are usually 5 km or larger, but detailed structures such as hail shafts may be a kilometer or less across. Since the fine scale maps have a resolution of 1 km, there is no point in asking for accuracy much better than 1 km. For ranges out to 60 km, this would require azimuth accuracy of ±0.6 degrees and range accuracy of ±700 m. A further point is that with the 1.6-degree beamwidth of the FPS 77, it would be difficult to detect azimuth errors smaller than 0.6 degrees. With 300-m range bins, 700-m range errors would be easily detectable.

7.1 Signal Calibration

7.1.1 RELATIVE CALIBRATION

Since there are no internal checks on the transmitted power and the receiver sensitivity in the FPS-77, one does worry that the system calibration may drift away from the normal, as components age. Fortunately, we have found that the radar returns from many of the topographic features (hills and small mountains) are stable, so that in fair weather we observe nearly the same values appearing on the digital charts from one map to the next and one day to the next. Thus, a procedure was set up to monitor the relative calibration by checking the returns from several ground targets. Ten grid locations were selected on the coarse scale map, in the WSW, NW, and NE directions, at ranges from 5 to 80 km. A series of four (or more) maps are obtained on fair weather days and an average of the 40 (or more) dB values is calculated. Individual values have a resolution of only 3 dB, but the average of forty or more points has a resolution of tenths of a dB. Calibrations attempted less than an hour after a rain storm usually produce averages 2 or 3 dB above the normal 38 dBZ_e, (presumably due to water drops remaining on trees and rocks) and are not considered valid.

Most of the calibration runs made are within 2.0 dB of the normal value, but once or twice a month, a value more than 2 dB too low will be found and a further check of the system is made. The most common trouble is with the receiver crystal, and is easily corrected by simple replacement. The system check is made with a signal generator, and at the same time a check of the log conversion

is also made. For proper range-normalization, the log strip must be kept close to specifications and there has been no difficulty keeping within ±0.5 dB.

This procedure for maintaining relative calibration is not perfect, as potentially serious calibration drifts (beyond 2 dB) have been detected on occasions when it was not feasible to make immediate correction, and as chance would have it, a storm followed soon afterwards. In such cases, corrections up to 4 dB have been applied to the data derived from archived digital maps, based on calibration checks before and after the storm. If more than 4 dB is needed, the data are not used, as there may be problems due to threshold of detection.

7.1.2 ABSOLUTE CALIBRATION

Without an absolute calibration, the radar-weather relationships developed from this system could not be applied to other radar systems. Several attempts at absolute calibration have been attempted, including the tracking of metal spheres attached to balloons as well as the placing of portable equipment within the radar beam. But due to a variety of difficulties, no attempt has been successful. The best that we have been able to do is to assemble simultaneous radar returns and rainfall rates and compute Z-R relations. By subtracting 20 dB from the radar values, we find a reasonably good fit to the relation formulated by Marshall and Palmer[9] from data collected at Montreal. Meteorologically, the rainstorms of Massachusetts and Montreal are similar and there is reason to believe that this procedure has produced an acceptable absolute calibration.

7.2 Position Calibration

When the first digital maps were produced by the program RADAR I, small, conspicuous ground targets were noted in most quadrants. Several of these features could be unambiguously identified as particular mountains or towers, and a check with available maps assured us that the horizontal positioning was correct to at least ±2 km. During the following two years, there were mechanical repairs made to the radar drive system, and after the last repairs we noted a change in the ground pattern on the digital maps. A small routine was then written to print out a string of any 29 consecutive range-bin values, every 0.4 degree of azimuth over a 24-degree sector. With the pulse integration set to a minimum, this routine allows precise positioning of towers and sharp summits, such as Grand Monadnock. We then found that the azimuth was off by 3 degrees, and we also found that the range was off by 600 meters, due to a misunderstanding about the format of the data stream produced in the data transmitter system. While these errors were not large, several cases were re-run with position corrections made, and we found no changes in the radar-weather relations. In October 1975, an adjustment was made in the synchro-to-digital converter to give correct azimuth, while a small modification was made to RADAR II to correct the range problem.

The elevation angle has not been thoroughly calibrated. We had hoped that by tracking a sphere attached to a balloon both by radar and double theodolites a calibration could be obtained, but two attempts failed. The only assurance we have that the elevation angles are reasonably correct, is that the vertical extent of distant thunderstorms (180 km or more in range) appear reasonable, which would not be the case if the elevation angle were off by more than one or two degrees.

8. SUMMARY

A versatile radar-computer system was installed at AFGL late in 1972 to answer the question of the utility of digital radar information in short-range aviation forecasting. Computer programs were written to provide digital maps to be used in real-time forecast experiments and to archive data for development of forecast aids. Preliminary studies of several wide-spread heavy rainstorms have produced inter-relationships between radar return, rainfall rate and extinction coefficient. Variations in drop-size distributions appear to reduce the capability of the radar in specifying extinction coefficient (ground level) and rainfall rate to an accuracy of about ±50 percent.

A technique has been developed to provide forecast assistance in the form of objectively determined motion vectors and guidance forecasts of severe weather parameters. On the first test, the forecast information appears to be useful and guidance forecasts were similar in accuracy to manual forecasts. However, more tests must be conducted before firm conclusions may be drawn.

Data collected during snowstorms will soon be analyzed to investigate the ability of radar to determine snowfall rates and the extinction coefficient in snow.

References

1. Hering, W.S., Muench, H.S., and Brown, H.A. (1972) Mesoscale forecasting experiments, Amer. Met. Soc. Bulletin, 53:1180-1183.
2. Wilson, J.W. (1970) Integration of radar and rain gauge data for improved rainfall measurement. J. Appl. Met. 9:489-497.
3. Tahnk, W.R. (1975) Objective Prediction of Fine-Scale Variations in Radiation Fog Intensity, AFCRL-TR-75-0264, p. 10.
4. Marshall, J.S., Langville, R.C., and Palmer, W. McK. (1946) Measurement of rainfall by radar, J. Meteor., 4:186-192.
5. Sekhon, R.S. and Srivastava, R.C. (1970) Snowsize spectra and radar reflectivity, J. Atmos. Sc., 27:299-307.
6. Donaldson, R.J., Chmela, A.C., and Shackford, C.R. (1960) Some behavior patterns of New England hailstorms. Physics of Precipitation, American Geophysical Union, Wash., DC, 354-368.
7. Weickmann, H.K. (1957) Physics of precipitation, Amer. Met. Soc. Meteorological Monographs, Vol. 3, No. 19, p. 228.
8. Middleton, W.E.K. (1952) Vision Through the Atmosphere, Toronto, University of Toronto Press.
9. Marshall, J.S. and Palmer, W. McK. (1948) The distribution of raindrops with size, J. Meteor., 5:165-166.
10. Ohtake, T. (1970) Factors affecting the size distribution of raindrops and snowflakes, J. Atmos. Sc., 27:804-813.
11. Waldvogel, A. (1974) The N_0 jump of the raindrop spectra, J. Atmos. Sc. 31:1067-1078.
12. Srivastava, R.C. (1967) On the role of coalescence between raindrops in shaping their size distribution, J. Atmos. Sc., 24:287-292.
13. Muench, H.S., Moroz, E.Y., and Jacobs, L.P. (1974) Development and calibration of the forward scatter visibility meter, AFCFL-TR-74-0145, Instrumentation Paper No. 217.

14. Marshall, J.S. and Gordon, W.E. (1957) Radiometeorology, Amer. Meteor. Soc., Meteorological Monographs, Vol. 3, No. 14, p. 96.

15. Wilson, J.W. and Pollock, D.M. (1974) Rainfall measurements during hurricane Agnes by three overlapping radar, J. Appl. Met., 13:835-844.

16. Blackmer, G.L., Duda, R.O., and Rebah, R. (1973) Application of Pattern Recognition Techniques for Digitized Radar, Final Report, Contract 1-36072, Stanford Res. Inst., Menlo Park, Calif.

17. Austin, G.L. and Bellon, A. (1974) The use of digital weather radar records for short-term precipitation forecasting, Quart. J. Roy. Met. Soc., 100:658-664.